

Tectonic control on the palaeogeographic evolution of thrust-top basins at the active margin of the Guadalquivir Basin (central Betic Cordillera, S Spain)

Julio Aguirre  | Juan C. Braga | José M. Martín | Ángel Puga-Bernabéu 

Dpto. Estratigrafía y Paleontología,
Facultad de Ciencias, Granada, Spain

Correspondence

Julio Aguirre, Dpto. Estratigrafía y
Paleontología, Facultad de Ciencias,
Avda. Fuentenueva s/n, Universidad de
Granada, Granada 18002, Spain.
Email: jaguirre@ugr.es

Funding information

Ministerio de Ciencia, Innovación
y Universidades/Agencia Estatal
de Investigación (MCIN/AEI),
Grant/Award Number: PID2022-
142806NB-I00 and PGC2018-099391-
B-I00; ERDF; Junta de Andalucía,
Grant/Award Number: RMN190

Abstract

The Guadalquivir Basin is the foreland basin of the Betic Cordillera (S Spain). Closest to the orogen, several thrust-top basins evolved during the Late Miocene in the central part of the cordillera. Here, we study the Upper Miocene deposits in five of these satellite basins: Montefrío, Iznájar-Cuevas de San Marcos, Antequera, Bobadilla Estación and Teba, in order to (1) update the stratigraphic framework, (2) infer a depositional model, (3) establish the relationship between sedimentary record and tectonic context and (4) reconstruct the palaeogeography of the area during the Late Miocene. Upper Miocene sediments mostly consist of mixed carbonate-terrigenous deposits. Facies characterization allows inferring a sedimentary model corresponding to a ramp with foreshore deposits changing to a shoal belt offshore in the inner ramp. Swaley and hummocky cross-stratified deposits formed in the transition to the middle ramp, and plane parallel carbonate beds in the distal middle-outer ramp. Factory facies, dominated by rhodoliths and bryozoans, also occur in the middle-outer ramp environments. Silts and marls formed in the deepest outer ramp and basin settings respectively. Breccias accumulated at the toe of palaeocliffs and conglomerates and massive coarse sands were deposited in fluvio-deltaic systems. Conglomerates and sands were also reworked as gravity flows and redeposited offshore. Local facies include rudstones-grainstones displaying large-scale trough-cross bedding formed in a strait in Montefrío, and marls with chalky carbonates deposited in a shallow marine, sheltered lagoon with hydromorphic soils in Bobadilla Estación. The study basins evolved in an N-S compressive tectonic context responsible of the emersion of the main Betic reliefs. Concomitantly, E-W and ESE-WNW extension originated the main depocentres. The influence of the tectonic activity on the sedimentary infills is indicated by the presence of synsedimentary deformations and several diachronic unconformities, which are younger westward. Tectonism, in turn, also controlled the palaeogeographic evolution during the late Tortonian-early Messinian interval.

This is an open access article under the terms of the [Creative Commons Attribution-NonCommercial-NoDerivs](https://creativecommons.org/licenses/by-nc-nd/4.0/) License, which permits use and distribution in any medium, provided the original work is properly cited, the use is non-commercial and no modifications or adaptations are made.

© 2024 The Authors. *Basin Research* published by International Association of Sedimentologists and European Association of Geoscientists and Engineers and John Wiley & Sons Ltd.

KEYWORDS

Foreland basin system, satellite basins, sedimentary-tectonic interplay, Tortonian-Messinian

1 | INTRODUCTION

The foreland basin systems embrace four zones, which from the orogen to the stable margin are called wedge-top, foredeep, forebulge and back-bulge depozones (DeCelles, 2012; DeCelles & Giles, 1996). Each depozone is characterized by different sedimentary infill geometries and subsidence histories directly influenced by the intricate processes taking place in the orogenic accretionary wedge (DeCelles, 2012; DeCelles & Giles, 1996). The wedge-top depozone is the geotectonic context where the so-called satellite (also termed piggyback or thrust-top) basins evolve (Bosence, 2005; Ingersoll, 2012; Ori & Friend, 1984). The sedimentary infill of satellite basins is usually characterized by significant clastic supply, synsedimentary deformations and frequent unconformities (Chen & He, 2022; Cheng et al., 2022; DeCelles, 2012; DeCelles & Giles, 1996; Hippolyte et al., 1994; Mutti et al., 2003). Wedge-top depozones are significantly interesting areas, as they record interactions between sedimentary accumulation and tectonic processes that structure the orogenic belt. Nonetheless, wedge-top basin deposits are exposed to intense erosion as a consequence of the tectonic uplift and, therefore, they are poorly represented except in the Mediterranean mountain ranges, where thick depositional sequences are preserved (DeCelles, 2012).

The Guadalquivir Basin (S Spain) is the foreland basin of the Betic Cordillera, in the western end of the Mediterranean (Figure 1a,f). It originated during the Miocene by the tectonic flexure of the passive Iberian southern palaeomargin as a consequence of the nappe stacking in the frontal wedge of the Betic Cordillera (García-Castellanos et al., 2002; Larrasoña et al., 2019). The southern active margin of the Guadalquivir Basin received large amounts of materials derived from the thrusting front, which are collectively called Guadalquivir allochthon (Flinch et al., 1996), frontal mélange unit (Pedrera et al., 2012; Ruiz-Constán et al., 2012), or Olistostromic Unit (e.g. Martínez del Olmo, 2019). As the orogeny advanced, the thrusting front acquired an irregular configuration and different basins and sub-basins developed associated with the emergent reliefs. They represent subsident areas in the wedge-top depozone, which evolved as satellite basins at the central southern margin of the Guadalquivir Basin during the Late Miocene (Jabaloy et al., 1992; Rodríguez-Fernández et al., 2012; Roldán & Rodríguez-Fernández, 1991; Ruiz-Constán et al., 2009; Sanz de Galdeano & Vera, 1992).

Highlights

- Late Tortonian-Messinian satellite basins evolved in the active margin of the Guadalquivir foreland Basin.
- The stratigraphic framework records the effects of the tectonic on the sedimentary infilling.
- Diachronic unconformities account for the tectonic activity in the Betic Cordillera orogen front.
- Drastic palaeogeographic changes took place in the region during the Late Miocene.

Numerous studies have focused on the sedimentary infill of the Guadalquivir Basin (e.g. Martínez del Olmo & Martín, 2016; Roldán, 1995; Sierra et al., 1996), on the tectonic evolution of the central-western Betic Cordillera (Galindo-Zaldívar et al., 2000; González-Castillo et al., 2015; Pedrera et al., 2012; Ruiz-Constán et al., 2012; Sanz de Galdeano, 1990), and on the origin and emplacement mechanisms of the Olistostromic Unit (e.g. Martínez del Olmo, 2019). Nonetheless, these studies analyse each aspect independently and mainly concentrated on the foredeep depozone of the Guadalquivir Basin. In addition, the Late Miocene sedimentary record of the basins closest to the orogenic front has been largely overlooked, except for a few regional works published in the last century (Cruz-Sanjulián, 1974; González-Donoso et al., 1980; Rodríguez-Fernández, 1982; Roldán, 1995; Serrano, 1979; Vera & González-Donoso, 1964).

In this study, the sedimentary, tectonic and palaeogeographic evolution of five satellite basins in the central Betic Cordillera are analysed in the context of the Guadalquivir foreland basin system evolution. This new approach is based on a better comprehensive biostratigraphic framework of the marine basin infills (Aguirre et al., 2022). The updated age model has allowed fitting the sedimentary evolution of the satellite basins with the compressive tectonism during the uplifting of the cordillera and precisating the palaeogeographic evolution during the Late Miocene. Previous studies indicated that marine sedimentation ended during the late Tortonian in some of the study areas, such as Antequera, Iznájar or Cuevas de San Marcos (e.g. Roldán, 1995; Serrano, 1979; van der Schee et al., 2018). Nonetheless, here we show that marine sedimentation continued up to the Messinian.

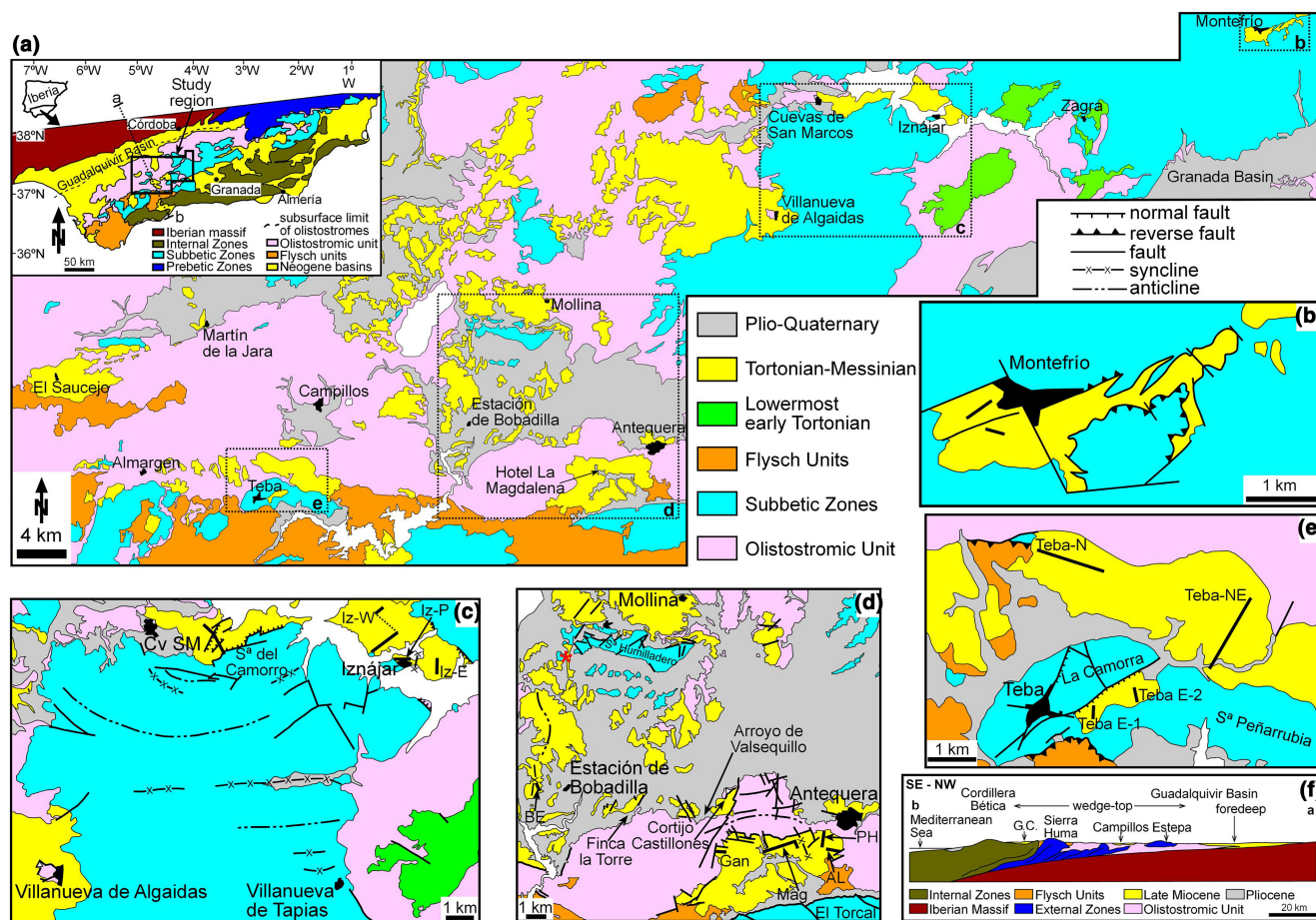


FIGURE 1 (a) Geological map of the study area. See location of the entire study area in the inset. Dashed rectangles delineate the detailed location of the different study areas. (b) Geological map of the Montefrío area with indication of the two study sections. (c) Geological map of the Iznájar-Cuevas de San Marcos area with indication of the study sections. Iz-W: Iznájar-W; Iz-P: Iznájar-Pueblo; Iz-E: Iznájar-E. (d) Geological map of the Antequera and Bobadilla Estación areas with indication of the study sections. BE: Bobadilla-Estación section; Gan: Gandigüela section; Mag: Magdalena section; PH: Pinar del Hacho section; AL: Arroyo Lagarto section. The red asterisk southwest of the Sierra del Humilladero ($37^{\circ}06'12.3''$ N – $4^{\circ}43'38.5''$ W) marks the location where the basal contact of the study Upper Miocene deposits is observed (shown in Figure 13a). (e) Geological map of the Teba area with indication of the study sections. (f) Geological section of the Guadalquivir foreland Basin. See location of the cross section in the inset in panel a. G.C., Guadalhore Corridor.

In addition, unconformities observed in different basins were considered coetaneous (González-Donoso et al., 1980; Rodríguez-Fernández, 1982; Serrano, 1979; Vera & González-Donoso, 1964), thus determining previous stratigraphic, tectonic and palaeogeographic interpretations. Here, we demonstrate that unconformities are not exactly coevals and we reconstruct the precise sedimentary evolution of each basin, which we relate with the regional and local tectonic contexts. Finally, the combined biostratigraphic, sedimentologic and tectonic approach have been crucial to establish the beginning and end of the Atlantic-Mediterranean connection through the Guadalhorce Corridor, which is capital to understand the Messinian palaeogeography and palaeoceanography of the Mediterranean.

The main objective of this paper is to study the sedimentary record in satellite basins of the central Betic

Cordillera, integrating it in the larger context of the Guadalquivir foreland basin evolution, in order to: (1) update their stratigraphic framework; (2) propose a depositional model for the infilling sediments and its relationship to the tectonic context and (3) infer the palaeogeographic evolution of the area during the Late Miocene.

2 | LOCATION AND GEOLOGICAL SETTING

The study area is located at the southern margin of the Guadalquivir foreland basin in the central Betic Cordillera (S Spain), which is the westernmost part of the peri-Mediterranean Alpine orogen (Figure 1a). It constitutes the northern branch of the Betic-Rifian arc. Three major tectonic domains are identified in the cordillera: (1) the

Internal Zones, formed by the superposition of three tectonic complexes, which are from bottom to top: the Nevado-Filábride Complex (Palaeozoic and older metamorphic rocks), the Alpujárride Complex (Palaeozoic to Mesozoic metasediments) and the Maláguide Complex (Palaeozoic-Miocene sediments) (Jabaloy et al., 2019); (2) the External Zones, a thrust belt composed of Mesozoic to Middle Miocene sediments deposited on the southern margin of the Iberian Massif (García-Hernández et al., 1980). The External Zones, in turn, are divided into the Prebetic Zone, closest to the Iberian palaeomargin and the Subbetic Zone, in a more distal position to the south and (3) the Flysch Units, composed of Upper Cretaceous to Middle Miocene allochthonous sandstones and silts accumulated in deep-sea fans (Jabaloy et al., 2019; Sanz de Galdeano & Vera, 1992). In addition to the foreland basin, several Late Miocene sedimentary intramontane basins evolved during the late orogenic stages and mountain uplift, some of them fossilizing the contact between the Internal and External Zones (Braga et al., 2002; Rodríguez-Fernández et al., 2012; Sanz de Galdeano & Vera, 1992).

At the southern active margin of the Guadalquivir foreland basin, the Olistostromic Unit embraces a tectonically complex chaotic pile of sediments dominated by soft and unconsolidated Triassic clays, sands, carbonates and gypsum, which include Cretaceous to Lower-Middle Miocene (Burdigalian-Langhian) materials from the External Zones (Roldán, 1995, 2009) (Figure 1a,f). The mechanisms involved in the emplacement and the age of the emplacement of the Olistostromic Unit (tectonics, diapiric domes, gravitational mass displacements), its surficial extension, as well as its internal organization are still debated (Berástegui et al., 1998; Flinch et al., 1996; Martínez del Olmo, 2019; Pérez-López & Sanz de Galdeano, 1994; Pérez-Valera et al., 2017; Rodríguez-Fernández et al., 2012, 2013; Roldán, 1995).

The Betic-Rif arc was formed by the westward collision of the Alborán Domain (Internal Zones) with the converging Iberian and African continents. The External Zones are a thin-skinned thrust belt, whose sediments were deformed by this collision during the Early-Middle Miocene originating west-northwest verging thrusts and folds (Platt et al., 2013). At the same time, crustal thinning in the Internal Zones generated extensional basins, including the Alborán Basin (Comas et al., 1999; Comas & Soto, 1999).

From the late Tortonian (Late Miocene) onward, the general compressional regime changed from WNW-ESE to approximately N-S due to the convergence of Africa and Eurasian plates (Galindo-Zaldívar et al., 2019). This N-S compression configured the main reliefs of the cordillera (Braga et al., 2003; Galindo-Zaldívar et al., 2019) including the uplift of major Subbetic reliefs as E-W to ENE-WSW

trending antiforms (Cano-Medina, 1991; Galindo-Zaldívar et al., 2003; Galindo-Zaldívar et al., 2019; Sanz de Galdeano & Alfaro, 2004). In addition, the N-S compression led to the north-northwestward extrusion of the olistostromic bodies into the foredeep depozone (Martínez del Olmo, 2019; Ruiz-Constán et al., 2012), creating an irregular basement of mostly Triassic materials over the study area. Concomitantly, NW-SE normal faults and E-W and NE-SW trending strike-slip faults shaped subsiding depocentres that acted as the major Late Neogene intermontane basins (Galindo-Zaldívar et al., 2019; Rodríguez-Fernández et al., 2012; Sanz de Galdeano & Vera, 1992). In the study area, closest to the orogen front, marine sediment accumulated in shallow-water satellite basins that evolved during the late Tortonian-Messinian.

3 | METHODS

In the first step, the outcrops assigned to the Late Miocene in the geological maps of the region (IGME: MAGNA 1:50,000) were examined. Five areas where these deposits are best exposed were selected (Figure 1a–e): (1) Montefrío, (2) Iznájar-Cuevas de San Marcos, (3) Antequera, (4) Bobadilla-Estación and (5) Teba. Stratigraphic sections were logged in each area (Figure 1b–e). Lithology, facies and structures were observed at the outcrop. Rock samples of the lithofacies distinguished based on field properties were collected in each section and 50 thin sections were prepared for petrographic characterization (Supporting Information). The relative abundance of terrigenous content and bioclastic components was estimated semiquantitatively using the comparison charts of Baccelle and Bosellini (1965). Regarding the biostratigraphic framework of the study areas, we follow the results obtained by González-Donoso et al. (1980) and Rodríguez-Fernández (1982) in Montefrío and by Aguirre et al. (2022) in the rest of the areas. The biostratigraphic results enable to integrate the depositional evolution, the main tectonic events structuring the basin infilling and the palaeogeographic evolution during the late Tortonian-Messinian interval in the study areas.

4 | LITHOFACIES DESCRIPTION AND INTERPRETATION

Carbonate and mixed terrigenous-carbonate deposits dominate the marine sedimentary record in the logged sections in all the study areas. Carbonate components in all lithofacies correspond to the heterozoan association (James, 1997). Thirteen lithofacies types have been differentiated (Table 1).

TABLE 1 Description of the features characterizing the described lithofacies.

Lithofacies	Description	Accessory structures	Major components	Accessory components	Palaeoenvironmental interpretation
Facies 1: Packstone-rudstone with planar, low-angle cross-stratification	Centimetre-scale beds displaying gently dipping cross-stratification	Relatively well sorting	Highly fragmented bioclasts (bivalves, bryozoans, benthic foraminifera)	Echinoids, coralline algae	Coastal, foreshore deposits
Facies 2: Packstone-rudstone with trough cross-stratification	Metre beds with pervasive trough cross-stratification (up to 3 m high)	Ubiquitous deformation and fluid scape structures. Terrigenous content up to 25%	Bryozoan fragments, trace fossils (<i>Bichordites</i> , <i>Scolicia</i> , <i>Thalassinoides</i> , <i>Ophiomorpha</i> , <i>Macaronichnus</i>)	Benthic foraminifera, echinoids, bivalves, barnacles, coralline algae	Shoal deposits formed in high-energy inner ramp
Facies 3: Packstone-rudstone with undulating cross-stratification	10- to 15-cm-thick beds with swaley-hummocky cross-stratification	Inner lamination seldom preserved	Bioclasts highly fragmented		Inner-mid ramp affected by storms
Facies 4: Bioclastic floatstone	Decimetre-to-metre massive beds		Well-preserved coralline algae, bryozoans		Mid-outer ramp. Factory facies
Facies 5: Plane bedded packstone	Up to 25-cm-thick fine-grained beds	Crude horizontal lamination. Terrigenous content >10%	Bryozoans, bivalves, benthic foraminifera	Echinoids, <i>Bichordites</i> trace fossil	Distal mid-outer ramp
Facies 6: Grainstone-rudstone with large trough cross-stratification	Decametric trough cross-stratification with internal smaller-scale (metre) trough cross-stratification	Terrigenous content up to 5%	Bryozoan fragments	Coralline algae, bivalves, benthic foraminifera, echinoids	Strait deposits
Facies 7: Breccias	Clast-supported angular granules to cobbles	Inverse grading. Coarse sandy matrix	Bivalve borings (<i>Gastrochaenolites</i>)	Barnacles, oysters (<i>Crassostrea</i>), bryozoans, rarely rhodoliths	Coastal cliff deposits
Facies 8: Conglomerates	Clast- or matrix-supported conglomerates. Centimetre to metre thick channelized beds	Packstone matrix. Normal and inverse grading. Structureless and cross-stratification. Amalgamation	Bivalve borings (<i>Gastrochaenolites</i>), oysters	Pectinids, bryozoans, echinoids	Fan-delta deposits in shallow settings. Gravity mass flow deposits due to storms or hyperpycnal hyperconcentrated flows in mid-outer ramp
Facies 9: Massive sandstones	Structureless coarse- to medium sandstones	Very rarely cross-bedding	<i>Bichordites</i> , <i>Scolicia</i> and <i>Thalassinoides</i> trace fossils		Fluvio-deltaic deposits

(continues)

TABLE 1 (Continued)

Lithofacies	Description	Accessory structures	Major components	Accessory components	Palaeoenvironmental interpretation
Facies 10: Bedded sandstones	Alternating cemented and non-cemented, cm-dm thick, beds	Trough- and undulating cross-lamination			Storm deposits in siliciclastic-dominated settings
Facies 11: Silts and fine sandstones	Massive cm-to-m thick beds	Massive	Planktonic foraminifera		Distal mid- to outer-ramp
Facies 12: Marls	Massive, homogeneous marls	Massive	Planktonic foraminifera		Basin deposits
Facies 13: Marls with carbonate nodules	Marls with nodules and thin beds (>10 cm thick) of chalky CaCO ₃	Massive	Shallow and O ₂ -depleted benthic foraminifera	Scarce planktonic foraminifera	Shallow, sheltered lagoon

4.1 | Facies 1. Packstone-rudstone with planar, low-angle stratification (Figure 2a)

This facies consists of sets of ca. 5-cm-thick beds displaying gently dipping unidirectional planar cross-stratification. Sediments are mostly composed of relatively well-sorted fragments of bryozoans, with bivalves, benthic foraminifera and coralline red algae as accompanying components. This facies is restricted to the base of the Upper Miocene deposits in the Montefrío area (Figure 1b).

4.2 | Interpretation

Facies 1 most likely represents foreshore beach deposits (Brenninkmeyer, 1982). Similar deposits have been described in other Neogene Betic basins (Braga et al., 1996, 2010; Martín et al., 1996).

4.3 | Facies 2. Packstone-rudstone with trough cross-stratification (Figure 2b)

This is the most extensively represented facies in the study areas. This facies is characterized by the ubiquitous presence of bidirectional trough cross-bedding up to 3 m high. Terrigenous content can be up to 25%. Major components are fragments of bryozoans, bivalves, barnacles, echinoids, coralline red algae and benthic foraminifera. Bioclasts are highly fragmented and abraded. Trace fossils, such as *Bichordites*, *Scolicia*, *Thalassinoides*, *Ophiomorpha* and *Macaronichnus*, are frequently observed.

Sedimentary structures are often deformed due to fluid escape and plastic deformation (sensu Chiarella et al., 2016). Deformed sedimentary structures include flame-like structures, as well as simple and complex folded-slumped foreset strata, and injectites (Figure 2c–e). Representative examples of intervals, several metres thick, of simple and complex folded-slumped foresets (sensu Allen, 1982) can be observed in the Montefrío, Bobadilla-Estación and Iznájar-Cuevas de San Marcos areas (Figure 2e). The former structures are simple recumbent foreset folds, while the latter involve several metres of superimposed buckled cross-strata showing numerous recumbent folds, occasionally faulted, due to downslope displacement of liquified sediment, as described by Allen (1982) and Chiarella et al. (2016). Both simple and complex plastic deformation structures occur in particular foresets sandwiched between undeformed trough cross-beds.

Occasionally, in the Iznájar-Cuevas de San Marcos area, sand dikes (injectites), up to 1 m long and from 10 to 30 cm wide are also observed (Figure 2d). They are composed of sandy carbonates similar to the enclosing sediments. These injectites show rectilinear margins with a

FIGURE 2 Different types of facies. (a) Panoramic view showing the contact between Facies 1, packstone-rudstone with planar, low-angle cross-stratification and Facies 2, packstone-rudstone with trough cross-stratification (Montefrío area). (b) Facies 2, packstone-rudstone with trough cross-stratification (Bobadilla Estación section). (c) Water escape structures (white arrows) (Iznájar-W section). (d) Sand injections (white arrows) (Iznájar-W section). (e) Deformed trough cross-bedding (Iznájar-W section). (f) Facies 3, packstone-rudstone with undulating cross-stratification (south of Cuevas de San Marcos section). (g) Facies 4, bioclastic floestone dominated by rhodoliths (Magdalena section). (h) Facies 5, vertical plane-bedded packstone (Teba-E section). The top of the section is to the right of the picture. (i) Facies 6, grainstone-rudstone with large trough cross-stratification (Montefrío area).



rough laminar banding parallel to the borders cut-crossing sandstones and calcarenites.

4.4 | Interpretation

The extensive Facies 2 represents shoal deposits formed in high-energy inner ramps. This lithofacies is common in other Neogene Betic basins forming a characteristic facies belt offshore the shoreline deposits (Betzler et al., 1997; Braga et al., 2006; Martín et al., 1996; Martín et al., 2004). The submarine dunes reflect bidirectional palaeocurrents, suggesting the influence of tides.

Water-escape structures are associated with trough cross-bedded packstone-rudstone that show alternating layers of

different grain size (Figure 2c). Coarser-grained layers include more pore water that tends to escape after shear stress or sediment overload and the squeezed water flows upward disturbing the cross bedding (Allen, 1982; Postman et al., 2009; Chiarella et al., 2016; Bhattacharaya & Saha, 2020).

Regarding the sandy carbonate injectites, the nearly vertical orientation of the dikes through the host deposits and their rectilinear borders (Figure 2d) indicate that the sediment mobilized across fractures (Hurst et al., 2011). The composition similar to the host rocks suggests that sediments are sourced from the inner ramp deposits. Sand emplacement is due to an increase in pore pressure and fluidization. Triggering mechanisms of fluidization and injection of sand usually are earthquakes (Obermeier, 1996), although they are not the only possible cause (Hurst

et al., 2011). The tectonic instability at the active basin margin suggests that seismic shaking is the most likely triggering mechanism for the observed sand injections.

Simple and complex deformation structures in the foresets can be triggered by sediment overload due to sudden sedimentation events, instability at the crest of dunes due to seismic shaking, pounding waves or shearing drag on liquified-liquidized sediments by subaqueous currents (Alfaro et al., 1997; Allen, 1982; Chiarella et al., 2016; Jones & Omoto, 2000; Owen & Moretti, 2011; Puga-Bernabéu et al., 2023; Shanmugam, 2021; Topal & Özkul, 2014). As for sand injections, earthquakes are the most likely triggering mechanism, which otherwise is the most common process generating soft-sediment deformation structures (Allen, 1982; Chiarella et al., 2016; Jones & Omoto, 2000; Shanmugam, 2021).

4.5 | Facies 3. Packstone-rudstone with undulating cross-stratification (Figure 2f)

This facies consists of 10- to 15-cm-thick beds showing undulating cross-stratification characterized by internal laminations displaying antiforms in the crests and swales in the valleys, typical of the swaley and hummocky cross-stratification. The lamination is often obscured and poorly observable. This facies is normally intercalated with Facies 4 and Facies 5 (see below).

4.6 | Interpretation

The sedimentary structures of Facies 3 are characteristics of storm deposits (Duke, 1985; Duke et al., 1991; Dumas & Arnot, 2006; Hunter & Clifton, 1982; Mount, 1982). They preferentially form offshore the shoal belt developed in the shoreface (Dott & Bourgeois, 1982; Dumas & Arnot, 2006). In the study areas, this facies intercalates either in Facies 2 (e.g. Pinar del Hacho and Magdalena sections) or in Facies 4 and 5 (e.g. lower unit in Montefrío). These relationships indicate deposition in transitional settings, from inner to middle ramp, close to the storm wave base. Similar deposits are represented in Middle Miocene carbonates in the Prebetic Zone, in which they form a facies belt approximately parallel to palaeoshoreline and offshore shoals (Braga et al., 2010).

4.7 | Facies 4. Bioclastic floatstone (Figure 2g)

This facies consists of decimetre-scale massive tabular beds (rarely up to 2m thick). These beds comprise large bioclasts, which are generally unbroken and well preserved,

embedded in a packstone matrix. Major components are coralline algae (both large isolated branches and rhodoliths) and bryozoans (both branches and nodules), accompanied by molluscs (oysters and pectinids), benthic foraminifera and echinoids. Nuclei of rhodoliths and nodular bryozoans are either fragments of other bioclasts (mostly bivalves) or lithoclasts (sandstones and limestones). Rhodoliths are built up by members of the order Hapalidiales (*Lithothamnion* spp. and *Mesophyllum* sp.) followed by members of the subfamily Lithophylloideae (mostly *Lithophyllum* group *incrustans*). This lithofacies is best represented in the Teba area, and it is generally restricted to thin intervals in other areas, such as Montefrío and Antequera (Figure 1b–d), where it occurs intercalated with Facies 3.

4.8 | Interpretation

Well preserved bioclasts embedded in a fine-grained matrix suggest deposition under relatively low-energy conditions in or nearby the production areas, that is, areas in which bryozoans, rhodoliths and other skeletal producers preferentially lived (factory facies of Martín et al., 1996). Dominance of the Hapalidiales as the major rhodolith-forming taxa indicates deposition in middle-outer ramp settings, at some tens of metres of water depth (Braga & Aguirre, 2001, 2004). In different Mediterranean- and Atlantic-linked Betic Neogene basins, similar factory facies accumulated offshore shoal systems (Aguirre & Braga, 2022; Braga et al., 2006; Martín et al., 1996, 2004; Puga-Bernabéu et al., 2007, 2008).

4.9 | Facies 5. Plane-bedded packstone (Figure 2h)

This facies is characterized by cemented thin-bedded, up to 25 cm thick, fine-grained carbonates mostly composed of fragments of bryozoans, bivalves and benthic foraminifera with varying amounts of terrigenous particles (less than 10% of the rock volume), mainly quartz grains. They frequently exhibit crude parallel lamination. Echinoid trace fossils (*Bichordites*) can be locally abundant. This facies typically occurs at the transition to Facies 11 and 12 (see below) in the upper part of the studied sections.

4.10 | Interpretation

Plane-bedded packstones (Facies 5) accumulated in low-energy, distal-middle to outer ramps. The crude horizontal lamination observed in this facies suggests that they formed due to sediment gravity flows. Similar lithofacies characterizes the distalmost deposits in carbonate ramps both in

Mediterranean-linked and Atlantic-linked Neogene basins of the Betic Cordillera (Puga-Bernabéu et al., 2014).

4.11 | Facies 6. Grainstone-rudstone with large-scale trough cross-stratification (Figure 2i)

This facies consists of 50–60% of bryozoan fragments with coralline red algae (up to 10%). Highly abraded fragments of echinoderms, bivalves and benthic foraminifera occur in lesser proportions. Terrigenous content is up to 5%. This facies shows by decametric trough cross-bedding, up to 20 m high and 50 m of lateral extension, and is exclusively present in the Montefrío area. Each set of mega cross-stratification is formed by beds, up to 50 cm thick, displaying smaller-scale bidirectional trough cross-bedding.

4.12 | Interpretation

The decametric dunes of Facies 6 are indicative of sediment movement under the action of strong currents. Submarine dunes of similar sizes form in extremely high-energy settings, such as in recent straits where the velocity of water masses increases substantially due to constriction of the cross-sectional area (Dalrymple, 2023; Longhitano, 2018; Rossi et al., 2023). Gigantic dunes of similar dimensions occur in other localities of the Betic Cordillera linked to ancient straits connecting the Atlantic and the Mediterranean Sea (Betzler et al., 2006; Martín et al., 2001, 2009, 2014; Puga-Bernabéu et al., 2023).

4.13 | Facies 7. Breccias (Figure 3a)

This facies includes clast- and matrix-supported angular granules to cobbles embedded in a very coarse-grained sandy matrix and showing inverse grading. Clasts are mostly composed of limestone, dolostone, marlstone, chert and sandstone. This facies is almost exclusively restricted to the base of the successions, such as in the Iznájar-E and Cuevas de San Marcos sections (Iznájar-Cuevas de San Marcos area), as well as in the Teba area. Carbonate clasts are often bored by bivalves (*Gastrochaenolites*). Very rarely, barnacles attached to clasts can be observed. Other fossils are fragments of large oyster shells (*Crassostrea*) and nodular colonies of bryozoans.

4.14 | Interpretation

The angular nature and size (centimetre to metre) of clasts in the breccia beds (Facies 7) indicate short transport from

the source areas. They are interpreted as rock-fall and debris-flow deposits at the toe of palaeocliffs and rocky shores in near-shore shallow settings (Braga et al., 2006; Martín et al., 2004, 2009). The presence of *Gastrochaenolites* generally evidences deposition in shallow marine waters (Bromley & Asgaard, 1993; de Gibert et al., 1998, 2012).

4.15 | Facies 8. Conglomerates (Figure 3b)

Conglomerates consist of clast- and matrix-supported granules to boulders made up of rounded clasts embedded in a packstone or sandy matrix. Major clast components are limestone, dolostones, marlstone, chert, quartzite and sandstone. Large pebbles of black micaschists are scarcely found in the Teba area. Conglomerates occur both as inverse- and as normal-graded channelized beds, which locally occur amalgamated, ranging from tens of centimetres up to 2 m in thickness. The beds can display cross-bedding. This facies occurs in all study areas intercalated either in carbonates of Facies 2 or in silts of Facies 11. Occasionally, carbonate clasts show bivalve borings (*Gastrochaenolites*), as well as oysters and barnacles attached to their surface. Fragments of pectinids, oysters, bryozoans, echinoderms and very rarely rhodoliths occur dispersed in the matrix.

4.16 | Interpretation

Clast composition in conglomerates (Facies 8) varies depending on the nature of the Betic substrate surrounding the different basins. These conglomerates are interpreted as fluvial discharges into the sea, as indicated by the presence of clasts encrusted by oysters and barnacles, as well as pectinids and other marine fossils dispersed in the matrix. Amalgamation of conglomerate beds also suggests deposition in shallow water close to the flow out point.

Occasionally, fine-grained matrix-supported conglomerates reached deeper settings, as erosive bodies interspersed in finer sediments such as silts and fine sandstones (Facies 11; see below). They can represent reworked conglomerates from shallower settings mobilized offshore by high-energy events, such as storms (Aguirre, 2000; Braga et al., 2006; Puga-Bernabéu et al., 2008, 2014). Capuano (1991) described similar deposits in the Pliocene conglomerates and coarse sands deposited in the Montecalvo in Foglia piggyback basin, NE Italy. Alternatively, they can be the result of hyperpycnal hyperconcentrated or concentrated flows crossing the ramp down to the middle-outer ramp from the emergent land (Mutti et al., 1996, 2003; Zabala, 2020). These deposits are typically associated with high-gradient small

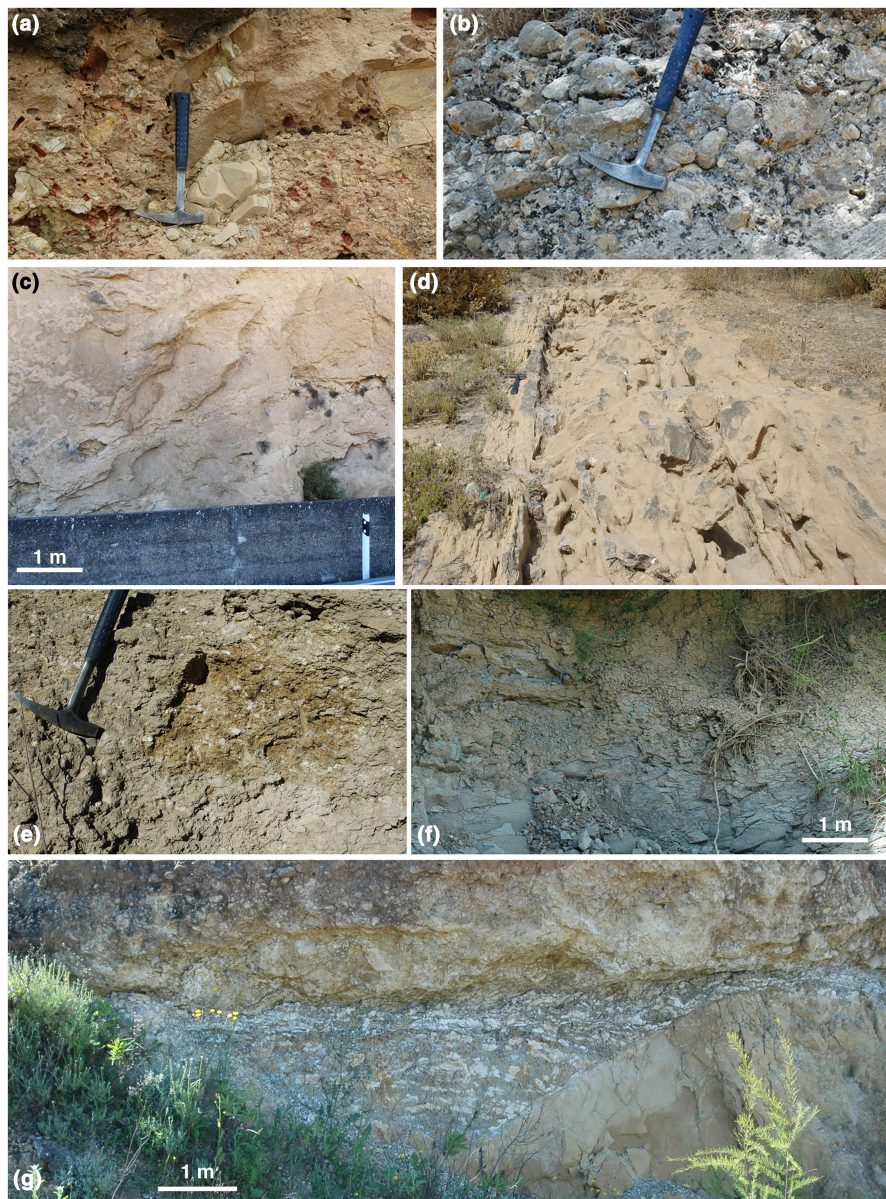


FIGURE 3 Different types of facies. (a) Facies 7, breccias (Iznájar-E section). (b) Facies 8, conglomerates. (Arroyo Lagarto section). (c) Facies 9, massive sandstones (Iznájar-Pueblo section). (d) Facies 10, bedded sandstones (Cuevas de San Marcos section). Strata are vertical and the top is to right of the picture. (e) Facies 11, silts and fine sandstones (Iznájar-Pueblo section). (f) Facies 12, marls (Magdalena section). (g) Facies 13, marls with white carbonate nodules (upper unit in Bobadilla Estación section).

rivers discharging sediments due to flash flows in marine shelves with steep slope (Zabala, 2020).

4.17 | Facies 9. Massive sandstones (Figure 3c)

It consists of structureless coarse to medium sandstones mainly composed of rounded quartz grains. This facies is restricted to the base of the Iznájar-Pueblo section (Iznájar-Cuevas de San Marcos area) (Figure 1c), forming a ca. 100-m-thick massive package. Large (up to 50 cm size) rip-up marly angular clasts derived from the Mesozoic substrate are incorporated into the sands at certain horizons. Sea urchin (*Bichordites*, *Scolicia*) and crustacean (*Thalassinoides*) trace fossils are seldom present.

4.18 | Interpretation

Facies 9 can be interpreted as sandy hyperpycnal flow deposits formed in fluvio-deltaic systems (sensu Mutti et al., 1996). These terrigenous deposits usually accumulated in tectonically active settings due to catastrophic floods from small mountainous high-gradient rivers discharging dense flows in narrow shelves (Milliman & Syvitski, 1992; Mutti et al., 1996, 2003; Zabala, 2020). Here, sediment-laden turbulent flows entering the basin can erode the substrate, incorporating rip-up clasts in the hyperpycnal flows (Mutti et al., 2003; Zabala, 2020). The thick interval of massive sandstones observed in the Iznájar-Pueblo section (ca. 100 m) suggests that fluvio-deltaic sands accumulated in a subsident narrow palaeotopographic embayment (see the palaeogeography section below) that acted as a trap of sediment. Similar thick massive sandstones deposited in

confined areas have been described in the Middle Jurassic Lotena Formation from the Neuquén Basin (Argentina) (Zabala, 2020).

4.19 | Facies 10. Bedded sandstones (Figure 3d)

This facies comprises alternating centimetre to decimetre-thick cemented and poorly cemented medium sandstone beds. Both types of beds show pervasive small to mid-scale trough cross-stratification and cross-lamination. Locally, swaley and hummocky cross-laminations are also observed.

4.20 | Interpretation

The alternating cemented and non-cemented bedded sandstones (Facies 10) are interpreted as storm beds (Duke, 1985; Dumas & Arnot, 2006; Hunter & Clifton, 1982). This facies is represented in the terrigenous-dominated deposits of the lower unit cropping out in the Cuevas de San Marcos section, where medium sands were reworked and transported by storms originating from discrete cemented sandy beds.

4.21 | Facies 11. Silts and fine sandstones (Figure 3e)

This facies involves massive silts and fine sandstones that locally intercalate channelized conglomerates (Facies 8) and plane-bedded packstones (Facies 5). *Bichordites* and *Thalassinoides* are often observed. It occurs in the upper part of the sections in most study areas. The vertical transitions of this facies are normally obscured due to cultivation, precluding detailed observations. This facies is also represented in centimetre-thick beds intercalated in massive sandstones (Facies 9; Iznájar-Pueblo section) and in cross-bedded packstone to rudstone (Facies 2; Arroyo Lagarto section).

4.22 | Interpretation

Facies 11 formed in distal-middle to outer ramp settings. In some sections, plane-bedded packstone beds (Facies 5) displaying incomplete Bouma sequences (Ta-Tb) intersperse in the silts supporting that episodic turbiditic sediment flows reached these distal settings. Turbidites are typical deposits in foreland basins formed after important uplifting events in the thrust and fold tectonic wedge (Mutti et al., 2003).

4.23 | Facies 12. Marls (Figure 3f)

This lithofacies consists of massive, homogeneous marls very rich in planktonic foraminifera and scattered bivalves and azooxanthellate corals.

4.24 | Interpretation

Marls of Facies 12 represent the deepest deposits and formed well below the storm wave base. The presence of abundant planktonic foraminifers corroborates deposition in deep-water conditions.

4.25 | Facies 13. Marls with chalky carbonate (Figure 3g)

This facies, exclusively present in the Bobadilla-Estación area (Figure 1d), embraces greenish marls with numerous chalky nodules and thin horizons (up to 10 cm thick and several metres in lateral extension) of calcium carbonate. Marls contain rich benthic foraminifer assemblages typically inhabiting oxygen-depleted, eutrophic settings (*Uvigerina*, *Rectuvigerina*, *Bolivina* and *Bulimina*) and shallow-water forms (*Ammonia beccarii*, *A. inflata*, *Elphidium* spp., *Asterigerinata planorbis*, *Lobatula lobatula*, *Cibicides* spp. and *Cibicoides* spp.). Planktonic foraminifera, although present, are scarce.

4.26 | Interpretation

The benthic foraminifer assemblages, together with the significant scarcity of planktonic forms and the type of sediment, are indicative of deposition in shallow, restricted conditions, most likely a marine sheltered lagoon (Murray, 2006). The chalky carbonates are interpreted as precipitated in hydromorphic soils developed in episodic desiccation events (Alonso-Zarza, 2003; Antisari et al., 2016; Zamanian et al., 2016).

5 | SEDIMENTARY MODEL

Spatiotemporal facies distribution in the different study areas allows establishing a general depositional model for a mixed carbonate-terrigenous ramp (Figure 4). Foreshore deposits (Facies 1) changed basinward and trough cross-bedded packstones-rudstones (Facies 2) accumulated in shoals on inner ramps. Shoal deposits prevail in the study areas indicating that these ramp settings were widespread throughout the entire region (Elez et al., 2016;

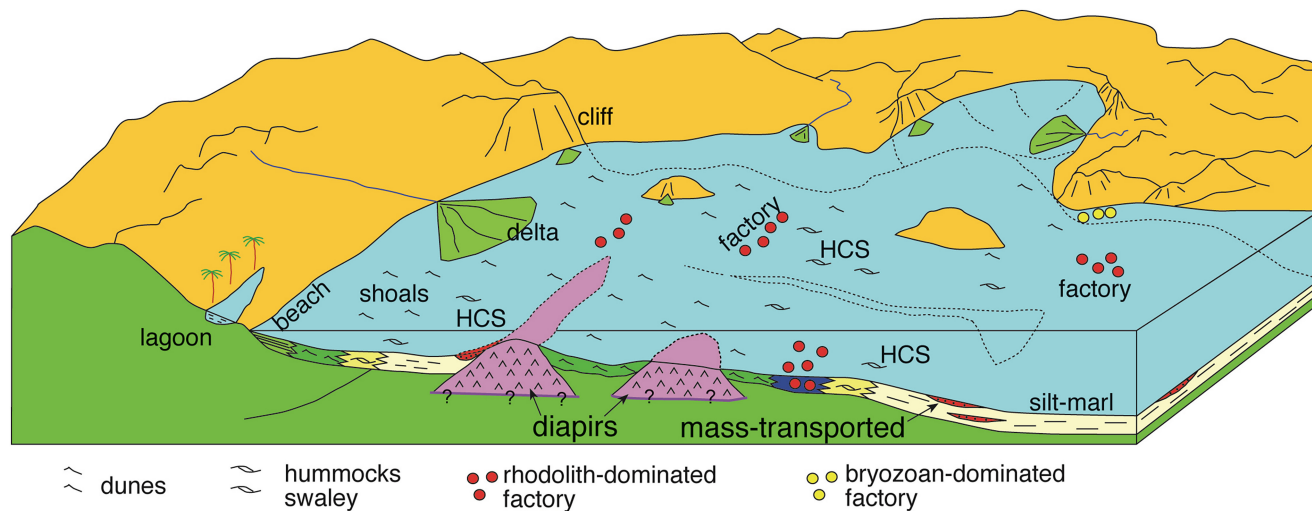


FIGURE 4 Schematic block diagram of the model proposed. (Not to scale). HCS: hummocky cross-stratification.

Martín-Serrano, 1986). Inner-ramp shoals changed offshore either to swaley and hummocky cross-stratified carbonates (Facies 3) or to plane-bedded carbonates (Facies 5) formed in deeper middle ramp environments. Factory facies (Facies 4) formed local patches distributed in the middle ramp and fed with bioclastic particles the shoals and the undulating cross-stratified carbonates. Offshore, sediments passed to outer ramp and basin silts and marls (Facies 11 and 12) with turbiditic tabular sandstone and packstone beds. Coarse terrigenous sediments accumulated in different contexts throughout the entire study areas. Breccias (Facies 7) were restricted to steep coastal settings whereas conglomerates (Facies 8) were associated with fluvial flows reaching from inner to outer ramp settings.

Within this general sedimentary model, which is valid for the different stratigraphic units recognized in the study areas, local conditions determined the deposition of a few facies in particular environmental contexts. This is the case of packstone-rudstone with large trough cross-stratification (Facies 6), only present in the upper unit of Montefrío, which formed in a narrow strait, and the marls with chalky carbonates (Facies 13), exclusively observed in the upper unit of Bobadilla-Estación, which was deposited in a shallow, sheltered lagoon.

6 | STRATIGRAPHIC ARCHITECTURE AND FACIES ARRANGEMENT IN THE STUDY AREAS

6.1 | Montefrío area

The Upper Miocene deposits overlie a Mesozoic to Middle Miocene basement and consist of two carbonate-dominated

units separated by an angular and erosive unconformity (González-Donoso et al., 1980; Rodríguez-Fernández, 1982; Vera & González-Donoso, 1964) (Figures 5 and 6a). The lower unit is intensively deformed showing vertical, and locally inverted strata (Figure 6a). This unit exhibits a deepening-upward succession. At the base of the unit, foreshore deposits (Facies 1) change southwestward to shoal deposits (Facies 2) indicating that the Montefrío basin opened in that direction. Shoal deposits, with deformation structures and extensive bioturbation by sea-urchin burrows (Figure 6b) also overlie Facies 1. Sedimentary structures show a southward (SW-SE) predominant palaeocurrents. Higher up in the section, Facies 2 intercalates floatstone beds (Facies 4) and hummocky-cross stratified deposits (Facies 3) (Figure 6c). The lower unit ends with thin plane-bedded packstone (Facies 5) intercalated in silts and marls (Facies 11 and 12). Planktonic foraminifer assemblages recovered in silts and marls at the top of the unit indicate an early Tortonian age (González-Donoso et al., 1980; Rodríguez-Fernández, 1982).

The upper unit starts with a conglomerate bed up to 0.75 m thick made up of pebbles to cobbles mostly derived from the underlying unit (Facies 8). The large-scale cross-stratified carbonates (Facies 6) above the conglomerate display a N60°E dominant palaeocurrent direction (Figure 6a). They represent submarine megadunes moved by water bottom outflow from the Mediterranean to the Atlantic, as in other Late Miocene straits in the Betic Cordillera (Betzler et al., 2006; Martín et al., 2001, 2009, 2014; Puga-Bernabéu et al., 2023). The foreset of smaller bedforms superimposed to the larger ones show bidirectional NE-SW palaeocurrents, indicating a tidal influence. These deposits have been attributed to the earliest late Tortonian based on the presence of *Globigerinoides extremus* and individuals close to *Neogloboquadrina humerosa* (González-Donoso et al., 1980; Rodríguez-Fernández, 1982).

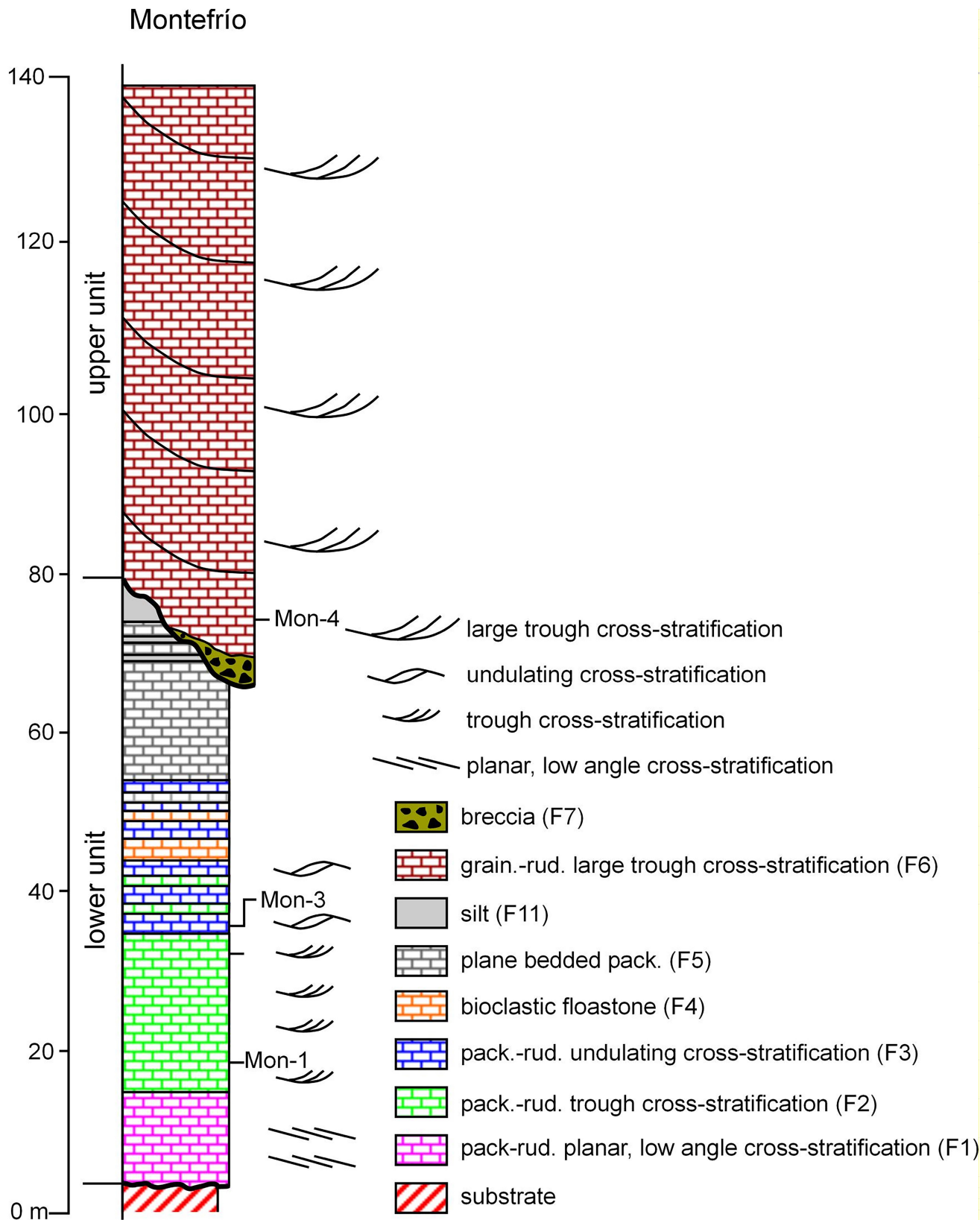


FIGURE 5 Composite stratigraphic column in the Montefrío area.



FIGURE 6 Montefrío area. (a) Panoramic view of the unconformity (dashed line). The lower unit is represented by vertical strata (white lines) and the upper unit is represented by large-scale trough cross-stratification. The white dashed line marks the limit between both units. (b) Beds of packstone-rudstone with trough cross-stratification of the lower unit showing intense bioturbation by sea urchins (*Bichordites* isp). (c) Panoramic view of the alternation of different facies.

6.2 | Iznájar-Cuevas de San Marcos area

The basement of the Upper Miocene deposits in this area comprises Jurassic limestones, dolostones and marlstones, as well as Triassic materials of the Olistostromic Unit (Figure 1c). One section between Serrezuela and Sierra del Camorro, ESE Cuevas de San Marcos (Cuevas de San Marcos section) (Figure 7), and three sections around Iznájar (Iznájar-E, Iznájar-Pueblo and Iznájar-W sections) (Figure 8) have been logged.

The Upper Miocene rocks consist of two unconformable units. The unconformity is conspicuous in Cuevas de San Marcos, where horizontal or gently dipping ($<10^\circ$) deposits of the upper unit overlie vertical strata of the lower unit (Figure 7). Here, the lower unit is intensely affected by jointing and faults that distort the succession and induce abrupt changes in dip and strike of strata. At the southeastern end of the Cuevas de San Marcos section, the lower unit shows a deepening upward trend. Shallow-water breccias and conglomerates at the base (Facies 7 and 8) change to bedded sandstones with undulating cross-lamination (Facies 10) and to silts and marls at the top (Facies 11 and 12) with tabular sandstone beds intercalated. Individual or amalgamated channelled conglomerates intercalate in these distal deposits.

The upper unit in Cuevas de San Marcos is dominated by breccias and conglomerates (Facies 7 and 8) made up of pebbles to cobbles derived from the basement and from carbonates of the lower unit (Figure 7). At the southern

margin of the section, the terrigenous deposits change upward to trough cross-bedded packstones-rudstones (Facies 2) and, finally, to silts and fine sands (Facies 11) (Figure 7). Sedimentary structures of Facies 2 show northward predominant palaeocurrents. Channelized conglomerates (Facies 8) intercalate in the carbonates as well as in the finer-grained sediments at the top of the unit.

In Iznájar, the unconformity is well exposed in the Cerro Cuchillo (Iznájar-W section) (Figure 9a), where the lower unit forms a NNW verging synform (Figure 9b). This unit is largely dominated by packstones-rudstones (Facies 2) with frequent intercalations of breccias and conglomerates (Facies 7 and 8), as well as massive sandstones (Facies 9) at its base. Trough cross-bedded packstones-rudstones (Facies 2) show an approximately E-W bidirectional palaeocurrents. In the Iznájar-W section, the middle-upper part of the unit is mostly dominated by channelized conglomerates (Facies 8) representing delta deposits intercalated within inner ramp carbonates (Facies 2). At the base of the Iznájar-E section, a thick interval of breccias derived from the basement abuts on the Jurassic basement rocks. Sediments fine progressively upward passing to silts (Facies 11) showing a deepening trend throughout the lower unit. Within this general trend, four successive intervals can be observed in the Iznájar-Pueblo section (Figure 9c). Each interval is characterized by a lower well-cemented thick-bedded portion and an upper poorly cemented thin-bedded set. The cemented sets stand out as prominent scarps in the landscape. These four intervals are interpreted as successive deepening-upward cycles.

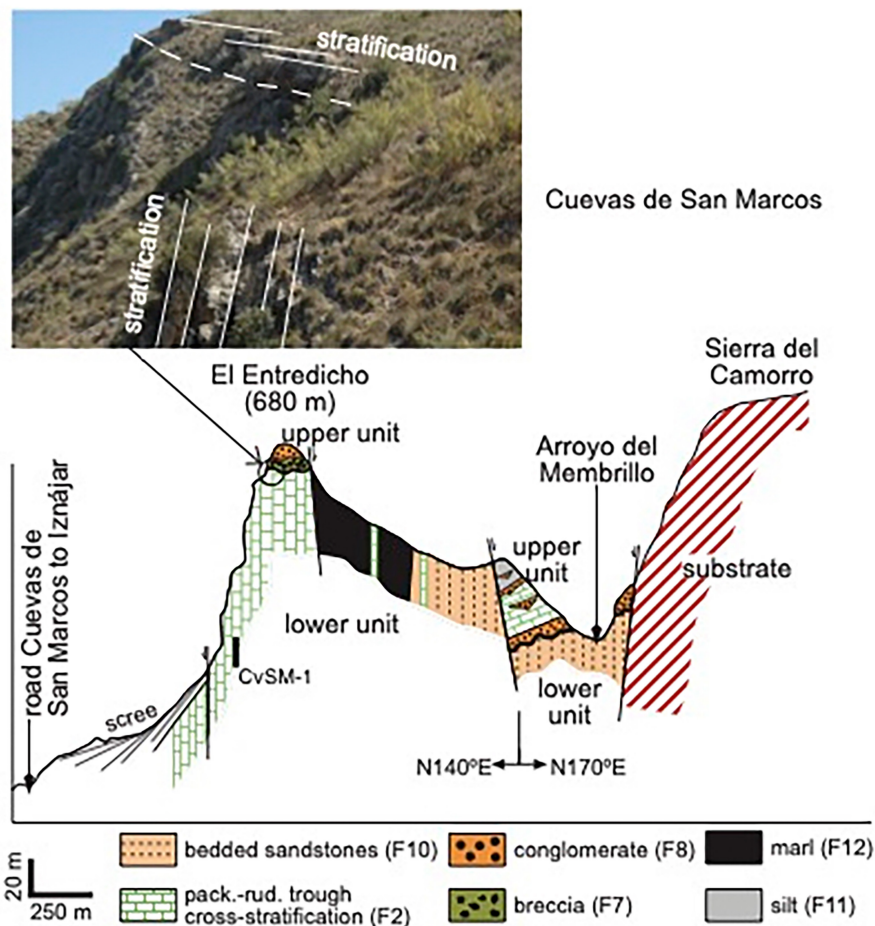


FIGURE 7 Cross section in Cuevas de San Marcos (base: $37^{\circ}15'41.3''$ N – $4^{\circ}23'43.1''$ W; top: $37^{\circ}15'30.4''$ N – $4^{\circ}23'13.4''$ W). The photograph shows a panoramic view of the unconformity (dashed line), with nearly horizontal strata of the upper unit overlaying nearly vertical ones of the lower unit (white lines).

An up to 0.5-m-thick conglomerate bed, including clasts eroded from the previous unit, lines the erosive surface at the base of the upper unit (Figure 9a). It mainly consists of packstones-rudstones with pervasive trough cross-bedding (Facies 2). In its upper part, silts and fine sands intercalate in the carbonates, and silts and marls occur at the top.

The lower unit in this area is late Tortonian and the upper one is Messinian in age (Aguirre et al., 2022).

6.3 | Antequera area

The study deposits are exposed immediately southwest of Antequera town, between Pinar del Hacho and Gandigüela (Figure 1d). There are other scattered outcrops distributed between the Antequera and the Bobadilla Estación areas (Figure 1d). Four stratigraphic sections were logged: two in the eastern sector, Arroyo Lagartos and Pinar del Hacho, one in the central part, Magdalena section, and one in the western sector, Gandigüela section (Figure 10). Between

the Magdalena and the Arroyo Lagarto sections, the Upper Miocene deposits form a southward verging syncline. The Upper Miocene deposits unconformably overlie Triassic materials of the Olistostromic Unit as well as marls and sandstones of the Flysch Units (Figure 11a). Triassic materials, in turn, locally overthrust Upper Miocene deposits, as seen south of Cortijo El Castellón, about 6 km W of Antequera (Figure 1d) (Martín-Serrano, 1986; Sanz de Galdeano et al., 2008). West of La Magdalena Hotel, a small outcrop of blue marls, early late Tortonian in age (Aguirre et al., 2022), is exposed (Figure 11b). These marls crop out only here precluding their in-depth analysis due to this limited areal distribution.

The rest of the Upper Miocene deposits, ranging from the late Tortonian to the early Messinian in age (Aguirre et al., 2022), overlie an erosive unconformity extensively bioturbated by *Thalassinoides* on top of the blue marls (Figure 11b). In the whole area, they are dominantly represented by packstones-rudstones with trough cross-stratification (Facies 2) that change upward to plane-bedded packstones (Facies 5), silts and fine sandstones

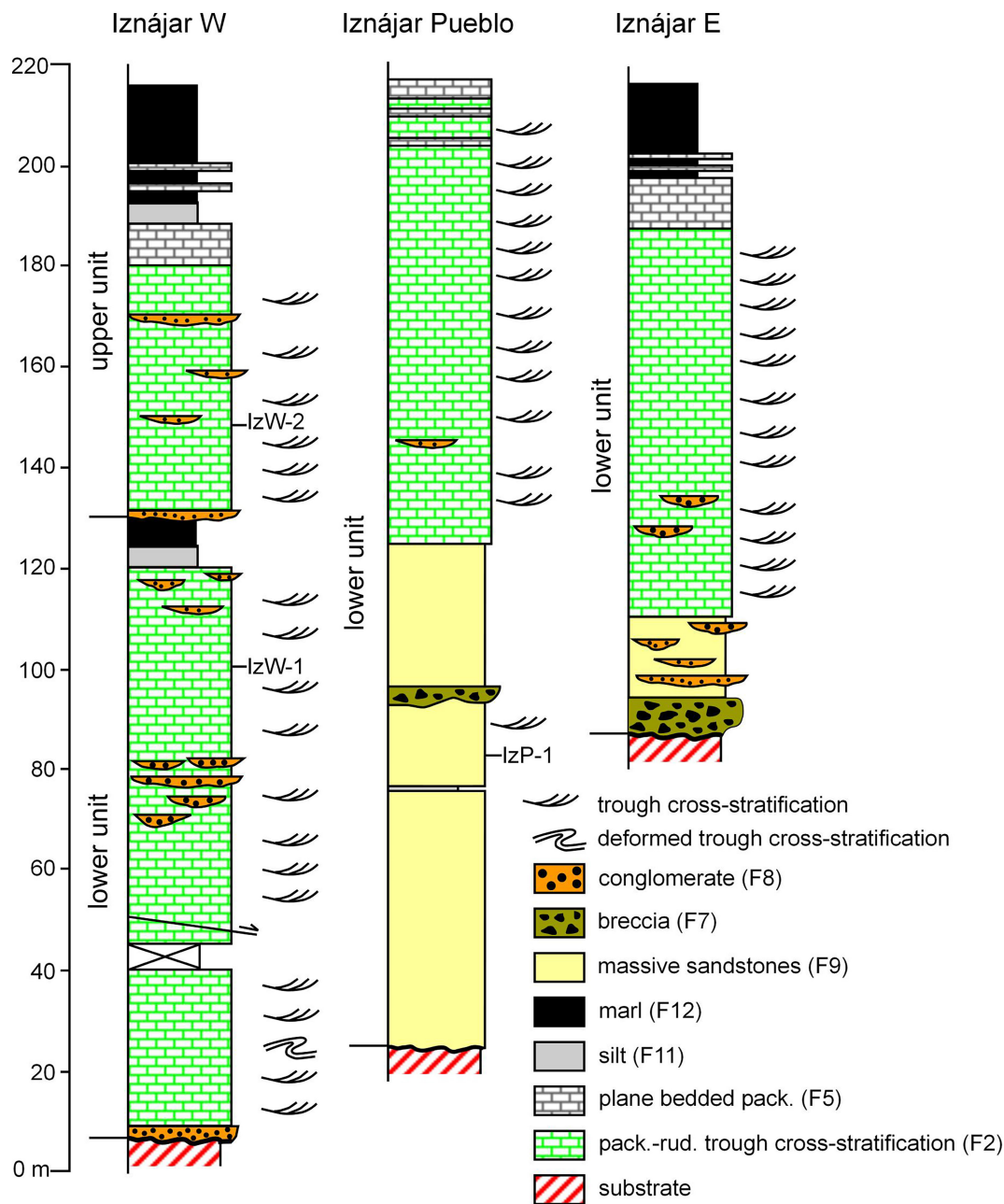


FIGURE 8 Stratigraphic sections in Iznájar. Iznájar W (base: 37°15'38" N – 4°19'03.2" W; top: 37°15'48.9" N – 4°18'56" W). Iznájar Pueblo (base: 37°15'28.8" N – 4°18'45.3" W; top: 37°15'32" N – 4°18'21.6" W). Iznájar E (base: 37°15'01.3" N – 4°17'45.7" W; top: 37°15'10.4" N – 4°17'43.4" W).

(Facies 11), and finally marls at the top of the sections (Facies 12) (Figure 10). In the easternmost Arroyo Lagarto and Pinar del Hacho sections, however, significant amounts of terrigenous sediments intercalate in the carbonates. Conglomerates (Facies 8) and less frequently breccias (Facies 7) occur at the base of the successions (Figure 10). Higher up in the sections, single channelized bodies or amalgamated beds of conglomerates (Facies 8) intercalate in the carbonates. In these two sections, the nature of the clasts changes vertically. In the lower 20 m, conglomerate clasts are made up of brownish sandstones, quartzites,

reddish marlstones, black dolostones and limestones. Clasts in the overlying conglomerate beds are almost exclusively of whitish limestones, minor brownish sandstones, and very rarely of quartz and chert. This indicates a shift in the source areas, from mostly Triassic materials of the Olistostromic Unit in the lower part to dominantly Jurassic carbonates of the El Torcal, located south of the area, in the upper part. Packstones-rudstones (Facies 2) are pervasively trough cross-bedded throughout the Arroyo Lagarto and Pinar del Hacho sections (Figure 10). Crude swaley and hummocky cross-stratification (Facies 3) is

FIGURE 9 Iznájár area.

(a) Panoramic view of Cerro Cuchillo showing the unconformity separating the two Upper Miocene units. The dashed line marks the boundary and the continuous white lines represent stratification. The inset shows a detail of the unconformity. (b) Panoramic view to the north of the Iznájár village showing folded strata of the lower unit. (c) Panoramic view of the Iznájár Pueblo section showing the four successive intervals. White arrows mark the well-cemented part of each interval.



locally present in the middle part of the Pinar del Hacho section. Channelized conglomerates (Facies 8) and plane-bedded packstone (Facies 5) beds intercalate in the silts and marls (Facies 11 and 12) at the top of the unit.

In the central and western sectors of the Antequera area, Magdalena and Gandigüela sections, respectively, terrigenous facies are nearly absent (Figure 10). A bed of rhodolith floatstone (Facies 4), up to 1 m thick, characterizes the base of the Magdalena section (Figure 2g). In the middle part of the section, an interval of plane-bedded packstones (Facies 5) and undulating cross-stratification (Facies 3) is observed (Figure 10). Channelized conglomerates intercalate in silts and marls at the top of the section (Figure 10). Marls are well developed at the top of the Gandigüela section (Figure 11c). Here, channelized conglomerates and plane sandy carbonate beds showing partial Bouma sequences intercalate in the marls (Figure 11d,e).

6.4 | Bobadilla-Estación area

The Bobadilla-Estación section was logged in an abandoned quarry west of Bobadilla railway station (Figures 1d and 12). The contact with the basement is exposed further to the north, west of the Sierra del Humilladero

(Figure 1d). Here, sandy packstones-rudstones with trough cross-bedding (Facies 2) fossilize an irregular surface, lined by breccias, carved in Upper Jurassic marls and marly limestones (Figure 13a).

The Miocene Bobadilla-Estación section consists of two unconformable units (Figures 12 and 13b). The lower unit can be divided in turn in two intervals. The lower interval consists of packstones-rudstones with pervasive trough cross-bedding displaying W-NW dominant palaeocurrents (N30°-70° W) (Facies 2) (Figure 13c) and the upper one is made up of silts and marls (Facies 11 and 12) (Figure 13b). Deformed cross-bedding and water-escape structures occur in the middle part of the carbonates in the lower interval. The transition from carbonates to the marls of the upper interval is gradual. The age of this unit ranges from late Tortonian to early Messinian (Aguirre et al., 2022).

The few planktonic foraminifers in the lagoonal marls of the upper unit suggest a Messinian age (Aguirre et al., 2022).

Well-cemented continental conglomerates occur erosively on top of the previous units (Figure 13b). These conglomerates crop out extensively in the Colonia de Santa Inés hamlet, along the road from Antequera to Campillos. The age of these conglomerates remains unknown, but they are most likely post-Messinian.

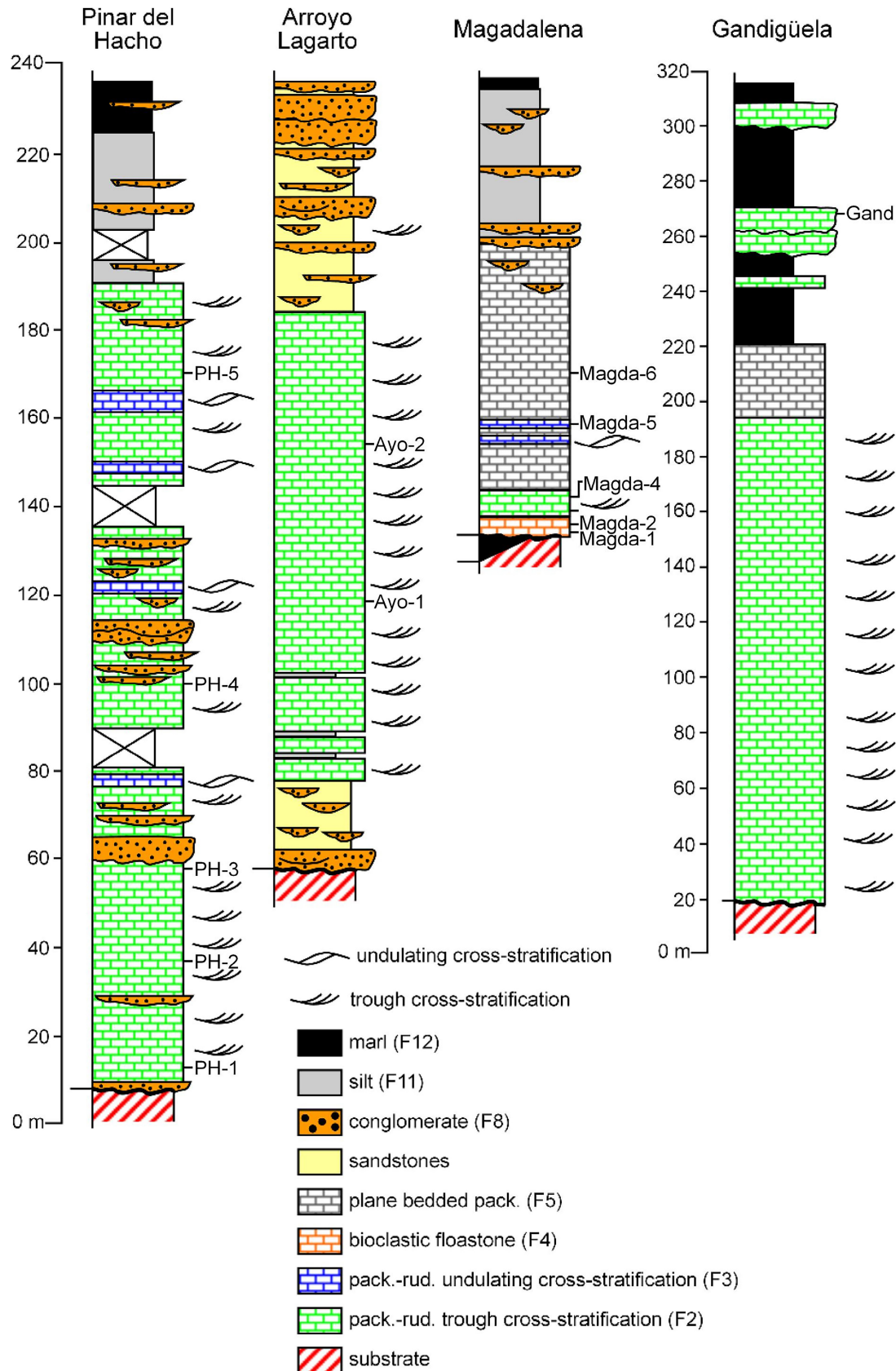
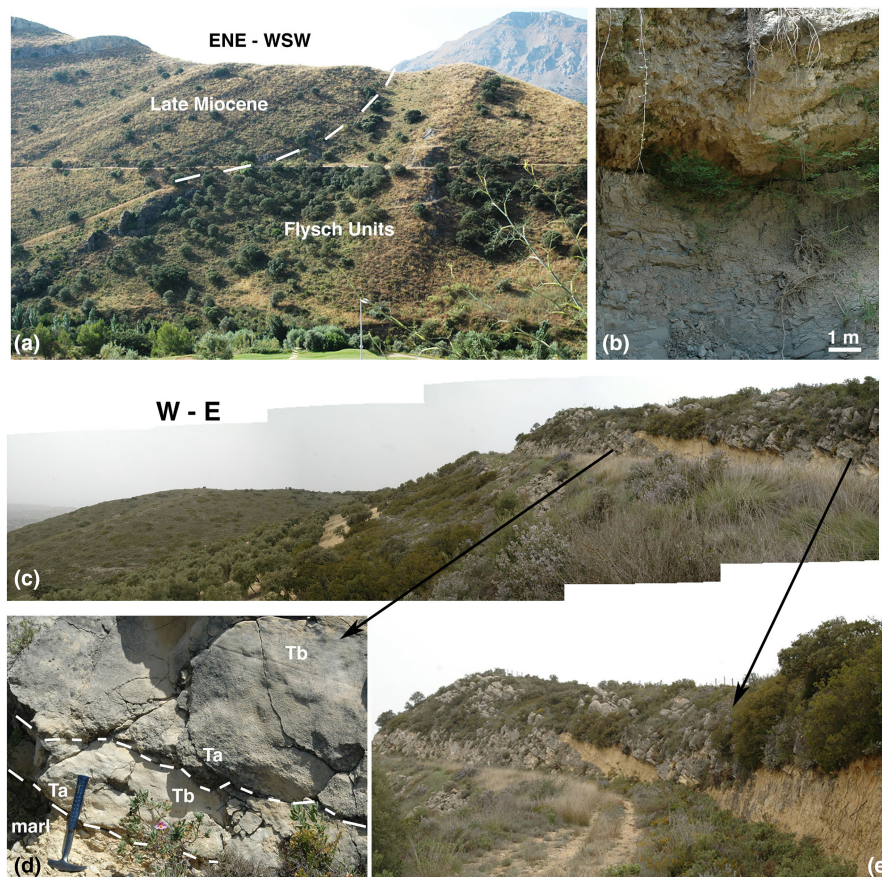


FIGURE 10 Stratigraphic sections in the Antequera area. Pinar del Hacho (base: $37^{\circ}00'45.9''$ N – $4^{\circ}34'14.0''$ W; top: $37^{\circ}00'26.0''$ N – $4^{\circ}34'18.8''$ W). Arroyo Lagarto (base: $37^{\circ}00'09.1''$ N – $4^{\circ}33'52.3''$ W; top: $37^{\circ}00'14.3''$ N – $4^{\circ}34'01.9''$ W). Magdalena (base: $37^{\circ}00'10.8''$ N – $4^{\circ}36'17.0''$ W; top: $37^{\circ}00'21.8''$ N – $4^{\circ}35'39.8''$ W). Gandigüela (base: $37^{\circ}00'15.3''$ N – $4^{\circ}38'07.2''$ W; top: $37^{\circ}00'14.1''$ N – $4^{\circ}37'24.9''$ W).

FIGURE 11 Antequera area. (a) Panoramic view of the contact between the Upper Miocene deposits and the substrate (Flysch Units) observed in Magdalena section. (b) Sharp contact between the blue marls (lower part of the late Tortonian) and the study upper Tortonian-lower Messinian unit. (c) Panoramic view of part of the Gandigiüela section. (d) Close-up view of two amalgamated turbidites, showing intervals Ta and Tb. (e) Channelized beds in the upper part of the Gandigiüela section intercalated in the marls.



6.5 | Teba area

Upper Miocene deposits crop out E and NNE of Teba (Figure 1e). Four stratigraphic sections have been logged: two E of Teba (Teba E-1 and Teba E-2) and two N and NE of the village (Teba-N and Teba-NE) (Figures 1e and 14). They unconformably cover the Olistostromic Unit to the north and east, as well as Jurassic and Cretaceous limestones and marlstones of the Sierra La Camorra and Sierra de Peñarrubia (Figure 13d).

East of Teba, the Upper Miocene deposits can be divided into two intervals: a lower one, badly exposed due to cultivation, and an upper interval dominantly consisting of trough-cross bedded packstones-rudstones (Facies 2), intercalating 15–60 cm thick of bryozoan floatstone beds and rhodolith floatstone beds (Facies 4) and 3–15-cm-thick plane-bedded packstones (Facies 5) with pervasive parallel lamination (Figure 14). Facies 4 is well represented in the upper part of the Teba E-2 section, close to the Sierra la Camorra (Figure 14). They are interpreted as deposits formed at the toe of submarine palaeocliffs, constituted by the Jurassic basement, similar to the bryozoan/coralline algal-dominated factory facies in the Tortonian deposits in the Cabo de Gata region (SE Spain) (Betzler et al., 2000).

In Teba-N, the Upper Miocene deposits are dominated by conglomerates made up of well-rounded clasts up to 15 cm

in diameter, arranged in decimetre-to-metre channelized beds and intercalating sandstones (Figure 14). Clasts are often bored by bivalves (*Gastrochaenolites*) or annelids and show attached oyster shells. These conglomerates fine eastward, passing to channelized conglomerate beds alternating with packstones-rudstones with trough cross-bedding (Facies 2). Further to the east (Teba-NE), these sediments grade to greenish-brownish marls (Figures 13d,e and 14).

Marls in the Teba-NE section (Figure 13e) contain abundant planktonic foraminifers and calcareous nannoplankton that unquestionably indicate basinal deposition during the early Messinian (Aguirre et al., 2022).

7 | DISCUSSION

7.1 | Sedimentation-tectonics interplay

The most conspicuous feature evidencing the control of tectonic processes on sedimentary evolution in wedge-top depozones is the presence of frequent unconformities, usually diachronic, triggered by reactivation events of the emerging reliefs in the orogen front (Beaumont, 1981; Chen & He, 2022; Cosovic et al., 2018; DeCelles & Giles, 1996; Kawakami, 2013; Mutti et al., 2003; Ori & Friend, 1984; Sinclair, 1997). In

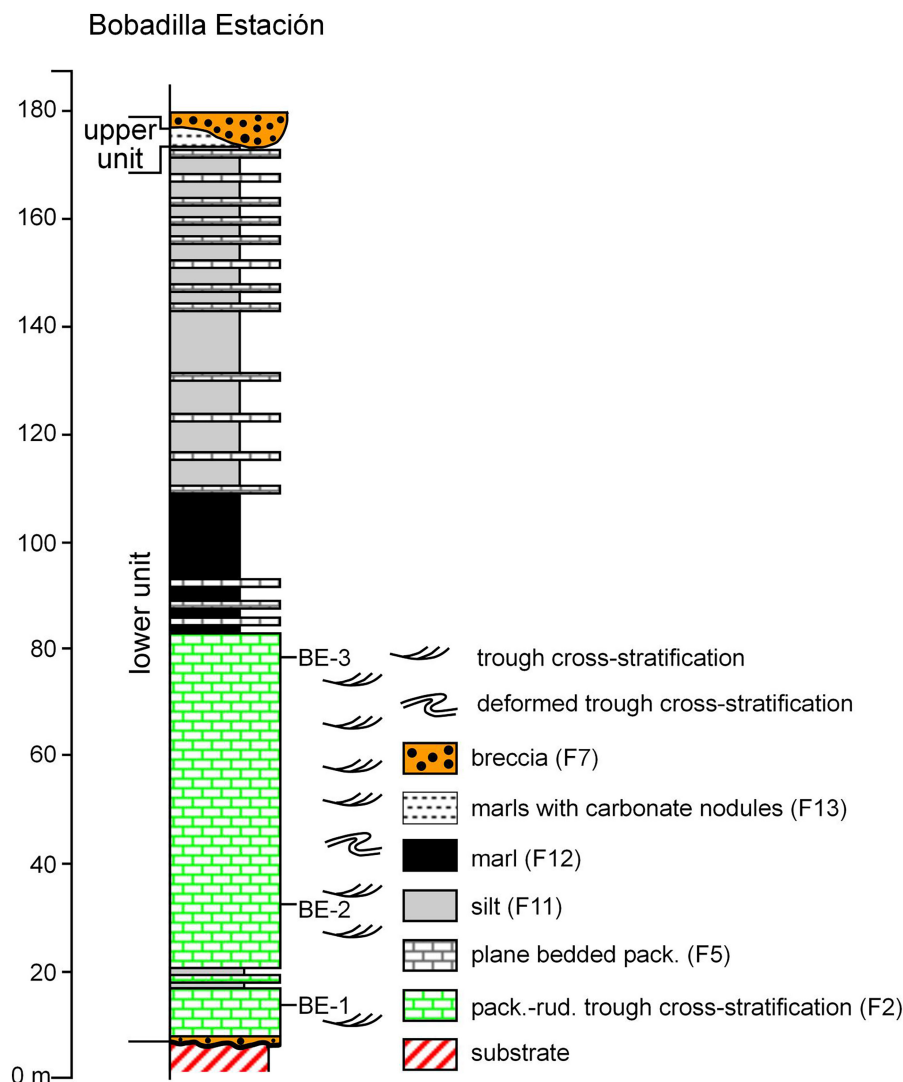


FIGURE 12 Stratigraphic section in the Bobadilla Estación area (base: 37°02'28.2" N – 4°45'00.2" W – top: 37°02'18.6" N – 4°44'54.1" W).

the central Betic Cordillera, during the late Tortonian, the tectonic regime was that of a nearly N-S compression due to the Eurasian-African convergence (Galindo-Zaldívar et al., 2019). This compression generated the main reliefs of the cordillera (Braga et al., 2003) and the north-northwestward extrusion of one of the olistostromic bodies (Ol-1 of Martínez del Olmo, 2019), or the late Tortonian olistostrome of Roldán (1995) into the fore-deep depozone (Figure 15).

In Montefrío, the tectonic event producing the unconformity separating the two Upper Miocene units took place close to the first occurrence of *Neogloboquadrina humerosa* (González-Donoso et al., 1980; Rodríguez-Fernández, 1982), which is 8.50 Ma, close to the MMi11 and MMi12 biozone boundary in the Mediterranean (Lirer et al., 2019). The topmost part of the blue marls in the Magdalena section (Antequera area) is earliest late Tortonian in age, also close to this biozonal boundary

(Aguirre et al., 2022). It is, therefore, reasonable to assume that the tectonic event producing the unconformity separating these blue marls from the overlying carbonates in Antequera could be closely coetaneous with that of the Montefrío (Unc-1 in Figure 15).

After this intra-Tortonian unconformity, the deposition of the upper unit in Montefrío during the late Tortonian occurred in a NE-SW elongated marine corridor, along one of the regional extensional fault systems. Following the closure of this corridor marine deposition ended in the Montefrío basin due to uplift (Lupiani-Moreno & Soria-Mingorance, 1985) (Figure 15). Oligocene marls locally overlie deposits of the two recognized Tortonian units in Montefrío. The crenulated outline of the reverse faults (Lupiani-Moreno & Soria-Mingorance, 1985) suggests a diapiric extrusion of marls, probably forced by compression.

In Antequera, the intra-Tortonian unconformity separating the blue marls from the overlying Upper Miocene



FIGURE 13 (a) Base of the lower unit of the Bobadilla Estación area as observed west of Sierra del Humilladero (red asterisk in Figure 1d). (b) Panoramic view of the top of the Bobadilla Estación section. The upper unit is sandwiched between the lower unit and the conglomerates. (c) Packstone-rudstone with trough cross-stratification (Facies 2) of the lower unit in Bobadilla Estación section. (d) Panoramic view of Teba-NE section (Teba area). Upper Miocene carbonates unconformably overlay the Jurassic basement (the dashed line follows the contact in this view). The carbonates change upward to marls, which crop out in the substrate of the olive trees. (e) Marls at the top of the Teba-NE section.

deposits marks an abrupt shift in the depositional conditions, from deep basinal to shallow-water ramp settings. Here, marine deposition of the upper unit continued up to the early Messinian (Aguirre et al., 2022) (Figure 15). North of the Antequera area, the Triassic materials formed an E-W elongated relief that supplied clastic materials as evidenced by the presence of Triassic clasts in the lower part of the Arroyo Lagarto and Pinar del Hacho sections. Subsequently, the Jurassic limestone in the antecedent relief of El Torcal at the southern margin of the basin, was the source of widespread terrigenous deposition in the southeastern sector of the basin during the late Tortonian (Martín-Serrano, 1986; Peyre, 1974).

The El Torcal is an ENE-WSW elongated relief formed by transpressive dextral displacements along strike-slip faults (Barcos et al., 2015; Sanz de Galdeano & López Garrido, 2012).

The Upper Miocene deposits in the Iznájar-Cuevas de San Marcos basin are limited by N320-325° E strike-slip faults and N60-65° E normal faults that favoured extension parallel to the major Subbetic reliefs surrounding the basin (Cano-Medina, 1990). During deposition of the lower unit in the late Tortonian (Figure 15), widespread terrigenous sedimentation from the basement prevailed in the whole area. In addition, syndimentary deformation structures are ubiquitous in the upper Tortonian

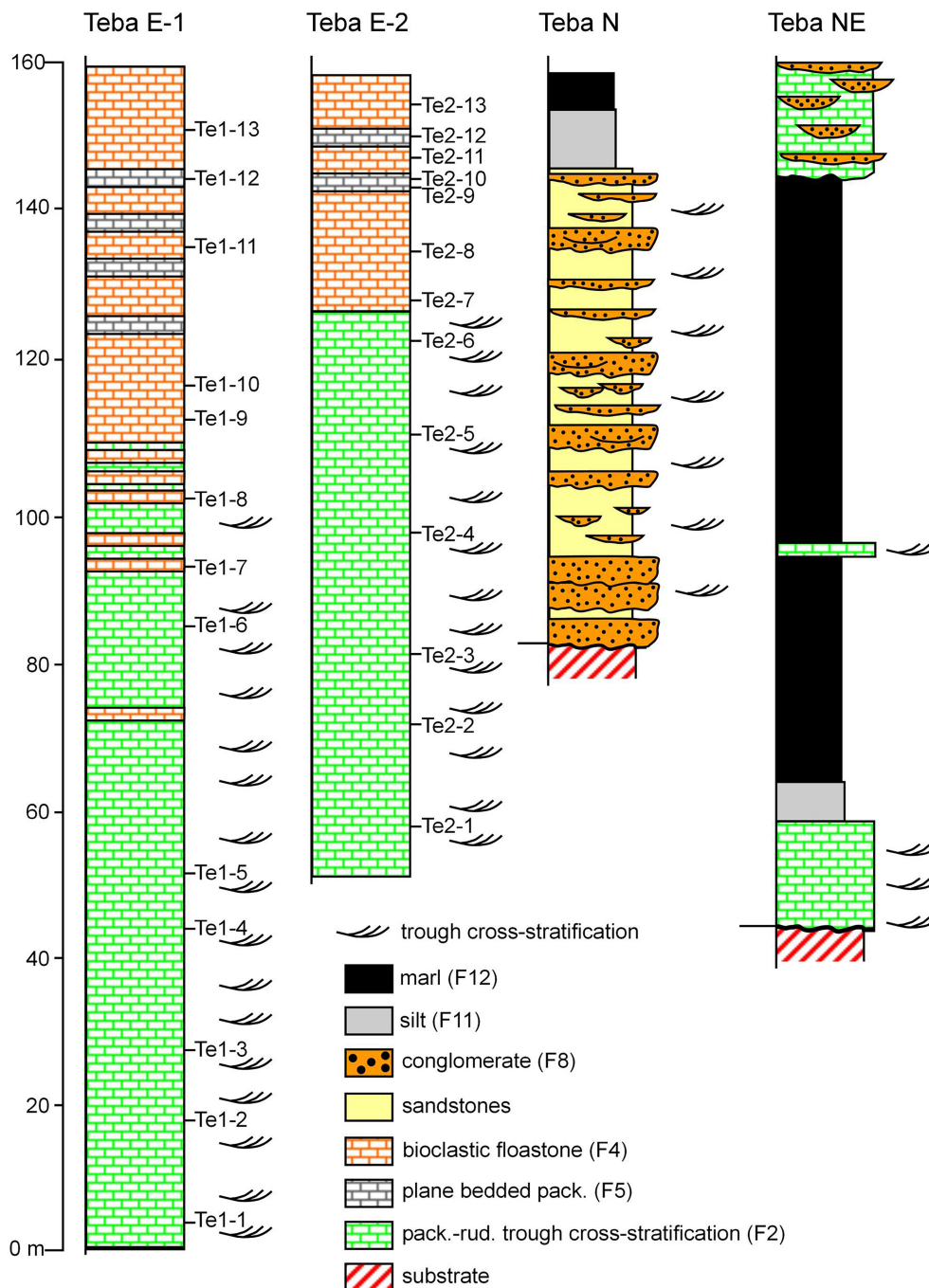


FIGURE 14 Stratigraphic sections in the Teba area. Teba E-1 (base: $36^{\circ}58'34.9''$ N – $4^{\circ}55'15.4''$ W; top: $36^{\circ}58'45.6''$ N – $4^{\circ}55'14.2''$ W). Teba E-2 (base: $36^{\circ}58'40.7''$ N – $4^{\circ}54'58.4''$ W; top: $36^{\circ}58'47.9''$ N – $4^{\circ}54'58.3''$ W). Teba-N (base: $37^{\circ}00'11.7''$ N – $4^{\circ}54'21.8''$ W; top: $37^{\circ}00'15.9''$ N – $4^{\circ}54'02.1''$ W). Teba-NE (base: $36^{\circ}59'18.4''$ N – $4^{\circ}52'53.7''$ W; top: $36^{\circ}59'44.7''$ N – $4^{\circ}52'10.1''$ W).

deposits. Both terrigenous deposition and generalized deformation are evident sedimentary expressions of tectonic activity of substrate adjacent to the wedge-top depozones (Beaumont, 1981; Chen & He, 2022; DeCelles & Giles, 1996; Fontana et al., 2015; Hippolyte et al., 1994; Ori & Friend, 1984; Sinclair, 1997). Clast composition indicates that the northern margin was mainly fed from the Olistostromic Unit, while the southeastern border was fed from Triassic reddish sandstones of the Olistostromic

Unit, as well as from Jurassic limestones and marly limestones of the Subbetic reliefs.

In the Iznájar-Cuevas de San Marcos basin, the tectonic event leading to the unconformity took place close to the Tortonian-Messinian boundary or during the earliest Messinian (Unc-2 in Figure 15). The upper Tortonian sediments of the lower unit were folded and uplifted due to the reactivation of the fault systems limiting the basin. Martínez del Olmo (2019) noted a

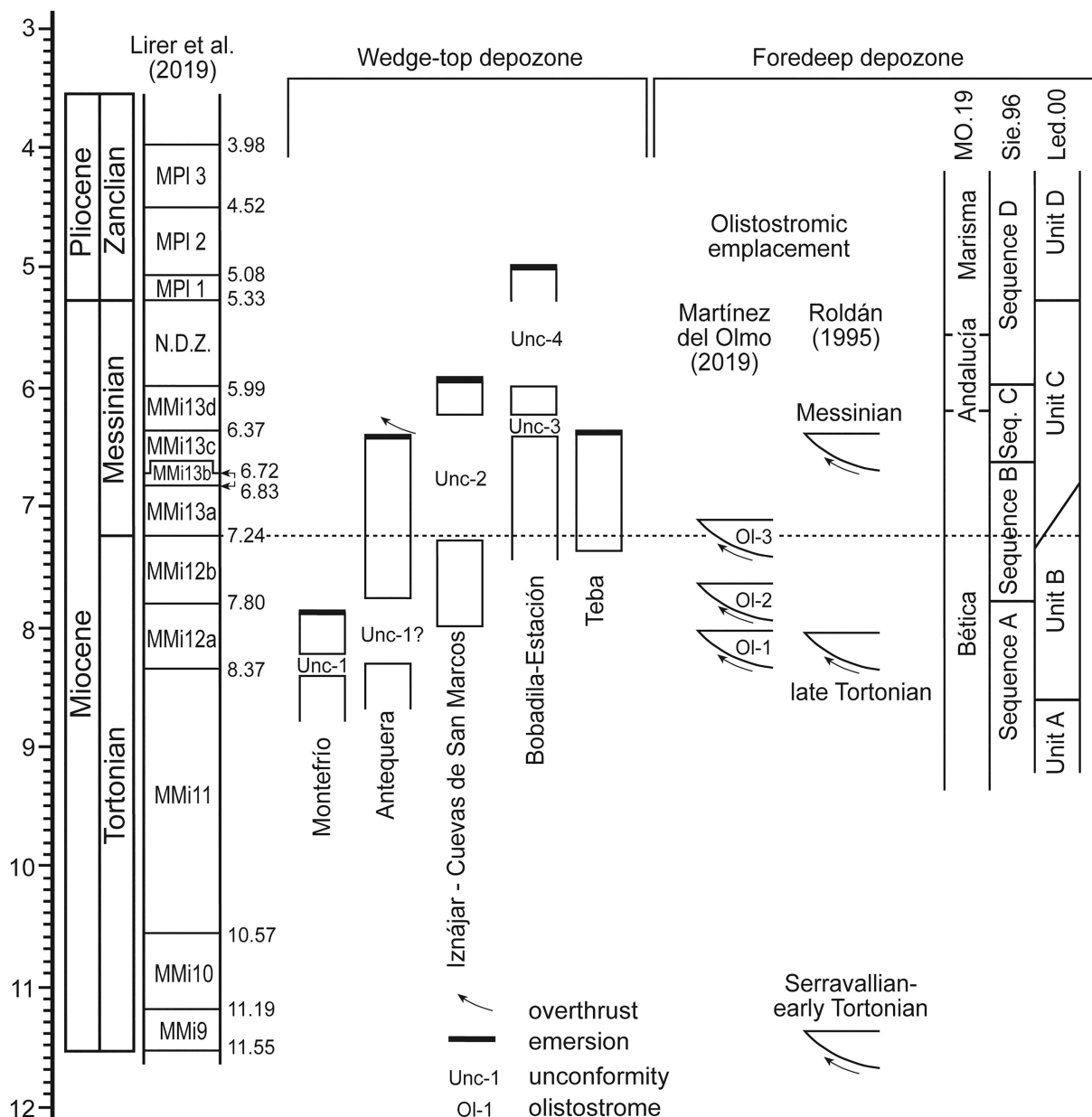


FIGURE 15 Summary chart of the stratigraphic framework of the study sub-basins in the wedge-top depozone of the Guadalquivir Basin compare with olistostromic deposits emplaced in the foredeep depozone. The stratigraphic division of the Upper Miocene deposits in the foredeep (at the right part of the figure) is based on different authors: MO.19: Martínez del Olmo (2019); Sie.96: Sierro et al. (1996); Led.00: Ledesma (2000). Unc-1 to Unc-4: Unconformities. OI-1 to OI-3: Olistostrome emplacements. Thick black lines indicate the final emersion of the different areas.

compressional event leading to the deposition of an olistostromic body (OI-3) in the foredeep depozone of the Guadalquivir Basin close to the Tortonian-Messinian boundary (Figure 15).

The continuous compressive regime led to the definitive emersion of the Antequera basin in the earliest Messinian (Figure 15). Here, the E-W trending Triassic materials cropping out north of Pinar del Hacho overthrust the Upper Miocene sediments in the Cortijo del Castellón (Martín-Serrano, 1986; Sanz de Galdeano et al., 2008). Between La Magdalena and Pinar del Hacho, south of this E-W

elongated Triassic outcrop, the Upper Miocene deposits are folded forming a southward-verging syncline and are markedly steepened close to the contact with the Triassic (Martín-Serrano, 1986). By contrast, north of the Triassic outcrop, between Antequera and Bobadilla-Estación (e.g. Finca La Torre, Arroyo de Valsequillo and Cortijo del Castellón) (Figure 1d), the Upper Miocene deposits dip to the north-northwest (Martín-Serrano, 1986). This structural arrangement on the northern and southern sides of the Triassic outcrop is consistent with a diapiric extrusion of the plastic Triassic materials (Martín-Serrano, 1986;

Sanz de Galdeano et al., 2008). In the eastern end of the Teba area, the vertical Upper Miocene beds at the contact with the Olistostromic Unit (Figure 2h), also suggest a diapiric uprising of the Triassic materials.

In the Bobadilla-Estación basin, the unconformity separating the two units is early Messinian (Unc-3 in Figure 15), since the lower unit ranges from the late Tortonian to the earliest Messinian and the upper one is early Messinian (Aguirre et al., 2022). Therefore, this tectonic event could be responsible for the final emersion of the Antequera basin commented above (Figure 15). An intra-Messinian unconformity has been also observed in the foredeep depozone of the Guadalquivir Basin (Ledesma, 2000; Martínez del Olmo et al., 1984; Martínez del Olmo & Martín, 2016; Sierro et al., 1996). This unconformity is linked to generalized uplift of the central Betic Cordillera leading to the emersion of most of the basins, such as the Granada and the Guadix-Baza basins. Related to this general uplift, the Guadalhorce Strait was definitively closed (Aguirre et al., 2022; Martín et al., 2001; Pérez-Asensio et al., 2012, 2013; Reolid et al., 2022) (Figure 15).

A similar Late Miocene sedimentary-tectonic interplay is inferred in the Rifian foreland basins, Saïss and Gharb basins (Bargach et al., 2004), in the southern branch of the Betic-Rifian mountain belt (N Morocco). These basins form an arcuate outline between the Rif fold-and-thrust orogenic front to the north and the Atlas to the south (Bargach et al., 2004; Roldán et al., 2014). As in the Guadalquivir foreland basin, several wedge-top basins evolved linked to the tectonically active Rif front during the late Tortonian-early Messinian interval (Abbassi et al., 2020; Achalhi et al., 2016; Di Staso et al., 2010; Roldán et al., 2014; Targhi et al., 2023). All these basins experienced tectonic shortening due to compression during the Late Miocene as indicated by the presence of unconformities and numerous synsedimentary deformation structures (Bargach et al., 2004; Chalouan et al., 2014; Roldán et al., 2014). The compressive tectonic regime led to the emersion and closure of the Rifian Corridors around the Tortonian-Messinian boundary, 7–7.2 Ma (Capella et al., 2018; Tulbure et al., 2017) or during the early Messinian (Abbassi et al., 2020; Achalhi et al., 2016; Chalouan et al., 2014; Di Staso et al., 2010; Targhi et al., 2023).

7.2 | Palaeogeographic evolution

During the Middle-Late Miocene, the Atlantic Ocean and the Mediterranean Sea were connected by several seaways (Martín et al., 2014). During the Serravallian, a wide passage developed in the southern Iberian palaeomargin (External Zones) between the Prebetic and Subbetic zones

(Braga et al., 2010; Martín et al., 2009). As the orogen front advanced, the passage evolved to a narrow strait, the so-called North-Betic Strait, which closed during the lowermost early Tortonian (Martín et al., 2009, 2014). The closure of this strait led to the individualization of the Guadalquivir Basin as an Atlantic-linked basin, although temporarily connected with the Mediterranean Sea through several straits that were closing during the Late Miocene as the uplift of the Betic Cordillera progressed (Betzler et al., 2006; Martín et al., 2001, 2009, 2014; Puga-Bernabéu et al., 2023) (Figure 16a).

As a consequence of the progressive uplift and emersion of the External Zones, the orogen front acquired a complex and irregular palaeogeographic configuration with different satellite basins among emergent uplands (Figure 16a). In addition, the emplacement of the Olistostromic Unit complicated the palaeogeographic evolution of this part of the central Betic Cordillera (Rodríguez-Fernández, 1982). This complex palaeogeographic outline, with different basins at different positions with respect to the orogen front and emergent islands in between, contrast with the late Tortonian-Messinian palaeogeographic models proposed by Roldán (1995), who established continuous WSW-ENE facies belts with satellite basins aligned parallel to that trend.

Depicting the detailed palaeogeography during the early Tortonian-earliest late Tortonian interval in the study region is difficult due to the scarcity of outcrops, except in the Montefrío area. Here, facies distribution indicates that there was a relatively narrow basin that opened to the west-southwest. Rodríguez-Fernández (1982) depicted a similar palaeogeographic configuration. In the Antequera area, the local presence of basinal marls at the base of the Magdalena section suggests the occurrence of a deep depocentre at the thrust front close to the early-late Tortonian boundary (Aguirre et al., 2022). These marls probably represent foredeep deposits in a previous stage during the thrust propagation in the orogenic front located further southwest of the Montefrío basin front.

The intra-Tortonian tectonic event led to significant palaeogeographic restructuring in the Montefrío area. Gigantic dunes in the upper unit suggest that a NE–SW trending strait connecting the Granada and Guadalquivir basins was active most likely during the earliest late Tortonian (Figure 16a). Continental sedimentation in the Granada Basin started in the latest Tortonian (late Turolian) and continued onward (Galindo-Zaldívar et al., 2019; García-Alix et al., 2008). This implies that the Montefrío strait was already closed by the late Tortonian and, therefore, its closure was approximately coeval with that of the Zagra Strait (Martín et al., 2014; Puga-Bernabéu et al., 2023) (Figure 16a,b).

During the late Tortonian, tectonics led to drastic palaeogeographic changes in the whole southern margin of the foreland basin (Figure 16b). By that time, the

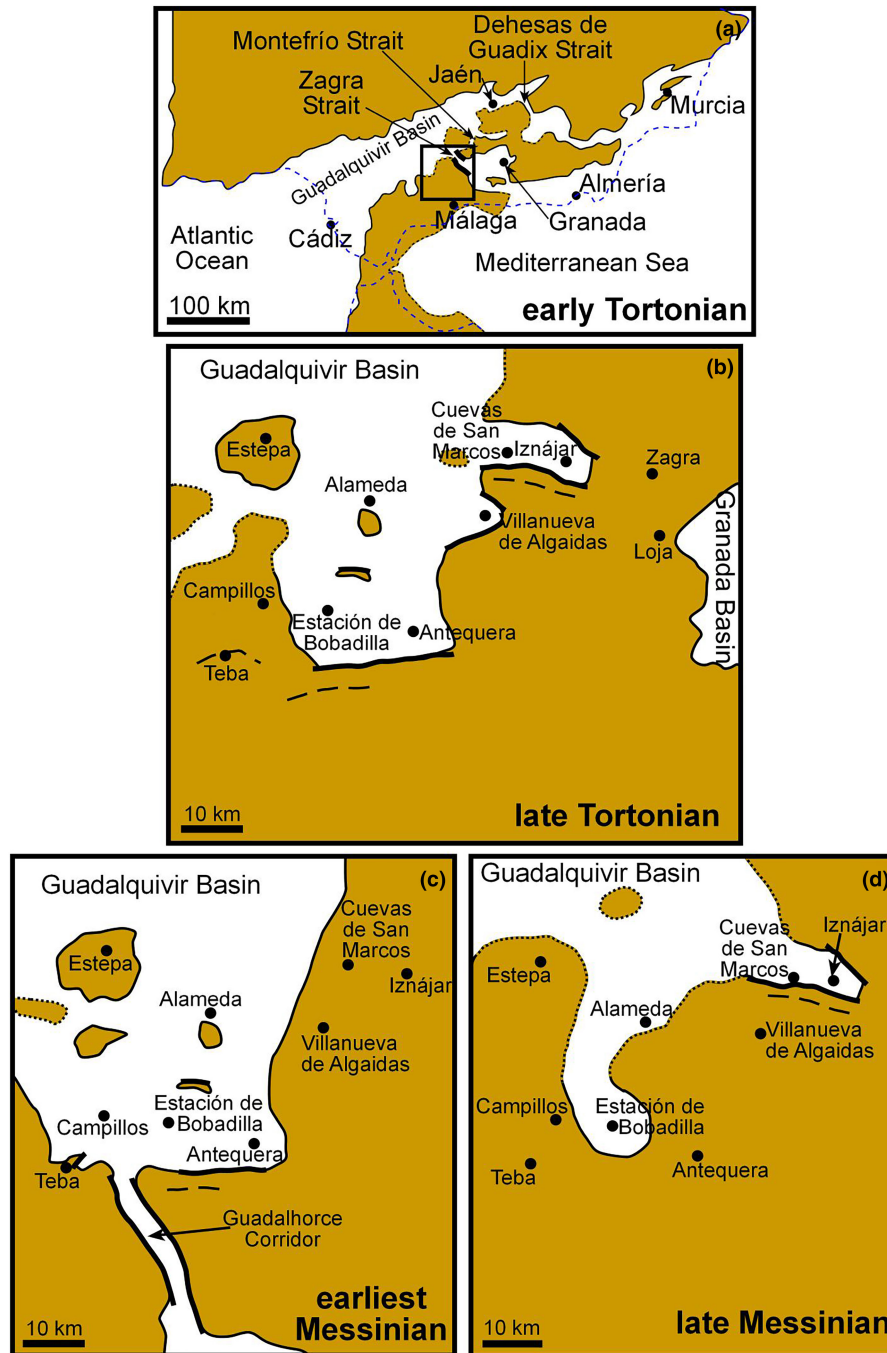


FIGURE 16 Palaeogeographic evolution of the study region. (a) Palaeogeography of the Betic Cordillera during the early Tortonian showing the straits connecting the Mediterranean and the Atlantic through the Guadalquivir Basin. The blue, dashed line depicts the present-day coastline. The square marks the area sketches in panels b to d. (b) Palaeogeography during the late Tortonian of the study areas. (c) Palaeogeographic outline during the lowermost early Messinian. Note that the Guadalquivir Corridor was open at this time. (d) Palaeogeography during the late Messinian. The Guadalquivir Corridor was closed during the lower Messinian and most of the study areas were definitively emerged except the Bobadilla Estación and Iznájar-Cuevas de San Marcos areas. Thick black lines in the four panels indicate major faults that controlled the palaeogeographic configuration in those satellite basins. Dashed black lines in panels b to d denote anticlines.

basement emerged as islands among subsiding depocentres in different positions relative to the Betic thrusts. The generalized uplift caused widespread shallow conditions in all these satellite basins (Elez et al., 2016).

Close to the Tortonian-Messinian boundary, uplift of the Iznájar-Cuevas de San Marcos area produced the tilting and emersion of the lower unit. Here, marine sedimentation resumed during the late Messinian (Aguirre

et al., 2022). Further to the southwest, however, earliest Messinian marine sedimentation continued in the Antequera, Bobadilla-Estación and Teba basins (Aguirre et al., 2022) (Figure 16c).

At the Tortonian-Messinian or during the lowermost early Messinian, the Guadalhorce Corridor opened following a palaeogeographic NW-SE trend coinciding with one of the major normal fault systems of the cordillera (Figure 16c). The aperture of this strait nearly coincided with the palaeogeographic shift leading to the emersion of the Iznájar-Cuevas de San Marcos area after the lower unit deposition. The corridor infill is a single depositional unit, which is laterally equivalent to the sediments in the Teba area, latest Tortonian-earliest Messinian in age (Aguirre et al., 2022). The palaeogeographic connection between the Teba area and the sediments in the Guadalhorce Corridor is also evidenced by the presence of micaschist pebbles in Teba-N section. The only possible source of these clasts are the metamorphic rocks in the Internal Zone lining the SW margin of the Guadalhorce Corridor (Cano-Medina, 1990). Peyre (1974) and Martín-Serrano (1986) also mentioned the presence of metamorphic granules and pebbles from the Internal Zone in the Cortijo del Castellón (WNW of Antequera) and close to Laguna de Fuente Piedra, west of Sierra del Humilladero (Figure 1a).

The intra-early Messinian tectonic event produced the closure of the Guadalhorce Corridor and the concomitant emersion of most of the region, except the Cuevas de San Marcos-Iznájar and Bobadilla-Estación areas (Figure 16d), where upper Messinian deposits are recorded (Aguirre et al., 2022).

In summary, the inferred palaeogeographic evolution shows a diachronic emersion of the different basins following an approximate westward component (Figure 15). An east-west component in the tectonic compression during the late Miocene is in agrees with geophysical data in the central and western sectors of the Betic Cordillera (González-Castillo et al., 2015).

8 | CONCLUSIONS

The Late Miocene stratigraphic architecture and sedimentary infilling of several satellite basins of the Guadalquivir foreland basin located close to the orogen front in the central Betic Cordillera have been studied. In addition, the relationship of the tectonic evolution of the orogen front and the sedimentary records in these basins has been analysed. Based on a comprehensive updated biochronostratigraphic framework, the results are integrated in the context of the Guadalquivir foreland basin system evolution and the generalized Late Miocene uplift of the central

Betic Cordillera in order to reconstruct the palaeogeography of the area during the late Tortonian-Messinian interval.

This study focuses on five areas: Montefrío, Cuevas de San Marcos-Iznájar, Antequera, Bobadilla Estación and Teba. The main conclusions are as follows:

1. The basins formed in an approximately N-S compression regime that led to the uplift of the main Betic reliefs, which constituted the basements of the sub-basins. A rough E-W extension controlled the formation of the depocentres. The overall N-S compression also led to the extrusion of the plastic Triassic materials, producing irregular basin bottoms and favouring widespread shallow marine deposition.
2. Different stratigraphic units separated by diachronic unconformities have been recognized in the satellite basins. An intra-Tortonian unconformity produced an important shift in the palaeoenvironmental conditions and sedimentary settings both in Montefrío and in Antequera basins. At the Tortonian-Messinian transition another unconformity is observed in the Cuevas de San Marcos-Iznájar area. Finally, an intra-Messinian unconformity is recorded in the Bobadilla Estación area. This diachronicity demonstrates that deposition of similar facies was also diachronic in the satellite basins, although in similar palaeoenvironmental contexts.
3. The sedimentary infill of the basins is characterized by carbonates and mixed terrigenous-carbonate deposits formed in a ramp. Foreshore deposits, distributed along the coastal areas, changed basinward to shoals formed in the inner ramp. Offshore, the shoals are laterally related with factory facies, plane-bedded carbonates or swaley and hummocky cross-stratified packstones-rudstones formed in storm-dominated mid-outer ramps. Silts and marls accumulated in the most distal outer ramp settings. Terrigenous sediments accumulated in different contexts throughout the study areas. Breccias were restricted to steep coastal palaeocliffs and conglomerates and coarse sands deposited in fluvio-deltaic systems. Conglomerates and coarse sands also deposited in deeper settings due to sediment gravity flows. Particular facies are grainstones-rudstones with decametric trough-cross bedding formed in a narrow, high-energy setting, most likely a corridor, in the Montefrío area. Greenish marls with white chalky carbonates accumulated in a sheltered, oxygen-depleted lagoon in Bobadilla Estación.
4. The tectonic activity in the orogen front also controlled the palaeogeographic changes. Emersion of the basins are diachronic, being younger westward, suggesting a tectonic compression that verges in that direction.

During the early-late Tortonian transition, a strait established in the Montefrío area. During the late Tortonian, the study area is characterized by an irregular outline, with wide embayments and emerged islands. The Guadalhorce Corridor opened at the Tortonian-Messinian boundary or during the lowermost early Messinian and closed during the early Messinian. During the late Messinian, marine sedimentation continued only in a shallow, oxygen-depleted enclosed lagoon in Bobadilla Estación, and in a WNW-ESE elongated embayment in Cuevas de San Marcos-Iznájar.

ACKNOWLEDGEMENTS

We thank Dr. Ayckbourn and an anonymous reviewer for their comments and suggestions to improve the quality of the paper. This research has been financed by the research projects PGC2018-099391-B-100 and PID2022-142806NB-100 funded by the Ministerio de Ciencia, Innovación y Universidades/Agencia Estatal de Investigación (MCIN/AEI)/10.13039/501100011033, and by ERDF A way of making Europe, by the European Union. We also acknowledge the support by the research group RMN190 of the Junta de Andalucía.

CONFLICT OF INTEREST STATEMENT

The authors have no conflict of interest.

PEER REVIEW


The peer review history for this article is available at <https://www.webofscience.com/api/gateway/wos/peer-review/10.1111/bre.12847>.

DATA AVAILABILITY STATEMENT

Data sharing is not applicable to this article as no new data were created or analysed in this study.

ORCID

Julio Aguirre  <https://orcid.org/0000-0002-7873-4544>

Ángel Puga-Bernabéu  <https://orcid.org/0000-0002-6420-9167>

REFERENCES

- Abbassi, A., Cipollari, P., Zaghoul, M. N., & Cosentino, D. (2020). The Rif chain (northern Morocco) in the late Tortonian-early Messinian tectonics of the Western Mediterranean orogenic belt: Evidence from the Tanger-Al Manzla wedge-top basin. *Tectonics*, *39*, e2020TC006164.
- Achalhi, M., Münch, P., Cornée, J. J., Azdimoussa, A., Melinte-Dobrinescu, M., Quillévéré, F., Drinia, H., Fauquette, S., Jiménez-Moreno, G., Marzeraud, G., Ben Moussa, A., El Kharim, Y., & Feddi, N. (2016). The late Miocene Mediterranean-Atlantic connections through the north Rifian corridor: New insights from the Boudinar and Arbaa Taourirt basins (northeastern Rif, Morocco). *Palaeogeography, Palaeoclimatology, Palaeoecology*, *459*, 131–152.
- Aguirre, J. (2000). Evolución paleoambiental y análisis secuencial de los depósitos plioceno de Almayate (Málaga, sur de España). *Revista de la Sociedad Geológica de España*, *13*, 431–443.
- Aguirre, J., & Braga, J. C. (2022). Middle Miocene (Serravallian) rhodoliths and coralline algal debris in carbonate ramps (Betic cordillera, S Spain). *Frontiers in Earth Science*, *10*, 958148. <https://doi.org/10.3389/feart.2022.958148>
- Aguirre, J., Braga, J. C., Martín-Pérez, J. A., Martín, J. M., & Puga-Bernabéu, Á. (2022). Upper Miocene deposits at the southern margin of the Guadalquivir Foreland Basin (central Betic cordillera, S. Spain). Implications for the closure timing of the Atlantic-Mediterranean connections. *Revue de Micropaleontologie*, *76*, 100690. <https://doi.org/10.1016/j.revmic.2022.100690>
- Alfaro, P., Moretti, M., & Soria, J. M. (1997). Soft-sediment deformation structures induced by earthquakes (seismites) in Pliocene lacustrine deposits (Guadix-Baza Basin, Central Betic Cordillera). *Eclogae Geologicae Helveticae*, *90*, 531–540.
- Allen, J. R. L. (1982). Sedimentary structures their character and physical basis. In J. R. L. Allen (Ed.), *Sedimentary structures. Their character and physical basis. Volume II. Developments in sedimentology* (Vol. 30B, pp. 343–393). Elsevier.
- Alonso-Zarza, A. M. (2003). Palaeoenvironmental significance of palustrine carbonates and calcretes in the geological record. *Earth-Science Reviews*, *60*, 261–298.
- Antisari, L. V., De Noboili, M., Ferronato, C., Natale, M., Pellegrini, E., & Vianello, G. (2016). Hydromorphic to subaqueous soils transitions in the central Grado lagoon (northern Adriatic Sea, Italy). *Estuarine, Coastal and Shelf Science*, *173*, 39–48.
- Baccelle, L., & Bosellini, A. (1965). Diagrammi per la stima visiva della composizione percentuale nelle rocche sedimentary. *Annali dell'Universita di Ferrara (Nuova Serie), Sezione 9. Science Geologia et Paleontologia*, *1*, 59–62.
- Barcos, L., Balanyá, J. C., Díaz-Azpiroz, M., Expósito, I., & Jiménez-Bonilla, A. (2015). Kinematics of the Torcal shear zone: Transpressional tectonics in a salient-recess transition at the northern Gibraltar arc. *Tectonophysics*, *663*, 62–77.
- Bargach, K., Ruano, P., Chabli, A., Galindo-Zaldívar, J., Chalouan, A., Jabaloy, A., Ahmamou, M., Sanz de Galdeano, C., & Benmakhlouf, M. (2004). Recent tectonic deformations and stresses in the frontal part of the Rif cordillera and the Saïss basin (Fes and Rabat regions, Morocco). *Pure and Applied Geophysics*, *161*, 521–540.
- Beaumont, C. (1981). Foreland basins. *Geophysical Journal International*, *65*, 291–329.
- Berástegui, X., Banks, C. J., Puig, C., Taberner, C., Waltham, D., & Fernández, M. (1998). Lateral diapiric emplacement of Triassic evaporites at the southern margin of the Guadalquivir Basin, Spain. In A. Mascle, C. Puigdefàbregas, H. P. Luterbacher, & M. Fernández (Eds.), *Cenozoic foreland basins of western Europe* (Vol. 134, 134, pp. 49, 49–68, 68). Geological Society of London, Special Publication.
- Betzler, C., Brachert, T. C., Braga, J. C., & Martín, J. M. (1997). Nearshore, temperate, carbonate depositional systems (lower Tortonian, Agua Amarga Basin, southern Spain): Implications for carbonate sequence stratigraphy. *Sedimentary Geology*, *113*, 27–53.

- Betzler, C., Braga, J. C., Martín, J. M., Sánchez-Almazo, I. M., & Lindhorst, S. (2006). Closure of a seaway: Stratigraphic record and facies (Guadix basin, southern Spain). *International Journal of Earth Sciences*, *95*, 903–910.
- Betzler, C., Martín, J. M., & Braga, J. C. (2000). Non-tropical carbonates related to rocky submarine cliffs (Miocene, Almería, southern Spain). *Sedimentary Geology*, *131*, 51–65.
- Bhattacharaya, B., & Saha, A. (2020). Large soft-sediment deformation structures (SSDS) in the Permian barren Measures Formation, Pranhita-Godavari Valley, India: Potential link to syn-rift palaeoearthquake events. *Journal of Palaeogeography*, *9*, 14. <https://doi.org/10.1186/s42501-020-00063-z>
- Bosence, D. W. J. (2005). A genetic classification of carbonate platforms based on their basinal and tectonic settings in the Cenozoic. *Sedimentary Geology*, *175*, 49–72.
- Braga, J. C., & Aguirre, J. (2001). Coralline algal assemblages in upper Neogene reef and temperate carbonates in southern Spain. *Palaeogeography, Palaeoclimatology, Palaeoecology*, *175*, 27–41.
- Braga, J. C., & Aguirre, J. (2004). Coralline algae indicate Pleistocene evolution from deep, open platform to outer barrier reef environments in the northern great barrier reef margin. *Coral Reefs*, *23*, 547–558.
- Braga, J. C., Martín, J. M., & Aguirre, J. (2002). Tertiary. Southern Spain. In W. Gibbons & T. Moreno (Eds.), *The geology of Spain* (pp. 320–327). Geological Society of London.
- Braga, J. C., Martín, J. M., Aguirre, J., Baird, C. D., Grunnaleite, I., Jensen, N. B., Puga-Bernabéu, Á., Saalen, G., & Talbot, M. R. (2010). Middle-Miocene (Serravallian) temperate carbonates in a seaway connecting the Atlantic Ocean and the Mediterranean Sea (north Betic Strait, S Spain). *Sedimentary Geology*, *225*, 19–33.
- Braga, J. C., Martín, J. M., Betzler, C., & Brachert, T. (1996). Miocene temperate carbonates in the Agua Amarga Basin (Almería, SE Spain). *Revista de la Sociedad Geológica de España*, *9*, 285–296.
- Braga, J. C., Martín, J. M., & Quesada, C. (2003). Patterns and average rates of late Neogene-recent uplift of the Betic cordillera, SE Spain. *Geomorphology*, *50*, 3–26.
- Braga, J. C., Martín, J. M., Riding, R., Aguirre, J., Sánchez-Almazo, I. M., & Dinarés-Turell, J. (2006). Testing models for the Messinian salinity crisis: The Messinian record in Almería, SE Spain. *Sedimentary Geology*, *188–189*, 131–154.
- Brenninkmeyer, B. (1982). Major beach features. In *Beaches and coastal geology. Encyclopedia of earth sciences series* (pp. 528–532). Springer. https://doi.org/10.1007/0-387-30843-1_268
- Bromley, R. G., & Asgaard, U. (1993). Endolithic community replacement on a Pliocene rocky coast. *Ichnos*, *2*, 93–116.
- Cano-Medina, F. (1990). *Rute. Segunda serie – Primera edición. Mapa geológico de España, escala 1:50.000*. Instituto Geológico y Minero de España.
- Cano-Medina, F. (1991). *Ardales. Segunda serie – Primera edición. Mapa geológico de España, escala 1:50.000*. Instituto Geológico y Minero de España.
- Capella, W., Barhoun, N., Flecker, R., Hilgen, F. J., Kouwenhoven, T., Matenco, L. C., Sierro, F. J., Tulbure, M. A., Yousfi, M. Z., & Krijgsman, W. (2018). Palaeogeographic evolution of the late Miocene Rifian corridor (Morocco): Reconstructions from surface and subsurface data. *Earth-Science Reviews*, *180*, 37–59.
- Capuano, N. (1991). Composition and provenance of the rudite and arenite facies in a foreland basin, northern Marchean Apennines, Italy. *Cuadernos de Geología Ibérica*, *15*, 185–207.
- Chalouan, A., Gil, A. J., Galindo-Zaldívar, J., Ahmamou, M., Ruano, P., de Lacy, M. C., Ruiz-Armenteros, A., Benmakhlouf, M., & Riguzzi, F. (2014). Active faulting in the frontal Rif cordillera (Fes region, Morocco): Constraints from GPS data. *Journal of Geodynamics*, *77*, 110–122.
- Chen, J., & He, D. (2022). Geometry, kinematics and mechanism of growth unconformities in the Biertuokuoyi piggy-back basin: Implications for episodic growth of the Pamir frontal thrust. *Journal of the Geological Society*, *179*, 16. <https://doi.org/10.1144/jgs2021-100>
- Cheng, F., Zuza, A. V., Liu, Y., & Sundell, K. (2022). Fold-and-thrust belts and associated basins: A perspective on their structure, sedimentation, and dynamics. *Journal of the Geological Society*, *180*, 4. <https://doi.org/10.1144/jgs2022-125>
- Chiarella, D., Moretil, M., Longhitano, S. G., & Muto, F. (2016). Deformed cross-stratified deposits in the early Pleistocene tidally-dominated Catanzaro strait-fill succession, Calabrian arc (southern Italy): Triggering mechanisms and environmental significance. *Sedimentary Geology*, *344*, 277–289.
- Comas, M. C., Platt, J. P., Soto, J. I., & Watts, A. B. (1999). The origin and tectonic history of the Alborán Basin: Insights from leg 161 results. In R. Zahn, M. C. Comas, & A. Klaus (Eds.), *Proceedings Ocean drilling program, scientific results* (Vol. 161, pp. 555–580). Ocean Drilling Program.
- Comas, M. C., & Soto, J. I. (1999). Brittle deformation in the metamorphic basement at site 976: Implications for middle Miocene extensional tectonics in the western Alborán basin. In R. Zahn, M. C. Comas, & A. Klaus (Eds.), *Proceedings Ocean drilling program, scientific results* (Vol. 161, pp. 331–334). Ocean Drilling Program.
- Cosovic, V., Mrinjek, E., Nemeč, W., Spanicek, J., & Terzic, K. (2018). Development of transient carbonate ramps in an evolving foreland basin. *Basin Research*, *30*, 746–765.
- Cruz-Sanjulián, J. J. (1974). *Estudio geológico del sector Cañete la Real – Teba – Osuna*. Ph.D. Thesis. Universidad de Granada.
- Dalrymple, R. W. (2023). A review of the morphology, physical processes and deposits of modern straits. In V. M. Rossi, S. G. Longhitano, C. Olariu, & F. Chiocci (Eds.), *Straits and seaways: Controls, processes and implications in modern and ancient systems* (Vol. 523, pp. 17–83). Geological Society of London, Special Publication. <https://doi.org/10.1144/SP523-2021-85>
- de Gibert, J. M., Domènech, R., & Martinell, J. (2012). Rocky shorelines. In D. Knaust & R. G. Bromley (Eds.), *Trace fossils as indicators of sedimentary environments. Developments in sedimentology* (Vol. 64, pp. 441–462). Elsevier.
- de Gibert, J. M., Martinell, J., & Domènech, R. (1998). *Entobia* ichnofacies in fossil rocky shores, lower Pliocene, northwestern Mediterranean. *PALAIOS*, *13*, 476–487.
- DeCelles, P. G. (2012). Foreland basin systems revisited: Variations in response to tectonic settings. In C. Busby & A. Azor (Eds.), *Tectonics of sedimentary basins: Recent advances*. Blackwell Publishing Ltd.
- DeCelles, P. G., & Giles, K. A. (1996). Foreland basin systems. *Basin Research*, *8*, 105–123.
- Di Staso, A., Perrone, V., Perrotta, S., Zaghoul, M. N., & Durand-Delga, M. (2010). Stratigraphy, age and petrography of the Beni Issef successions (external Rif, Morocco): Insights for the

- evolution of the Maghreb chain. *Comptes Rendus Geoscience*, 342, 718–730.
- Dott, R. J., & Bourgeois, J. (1982). Hummocky stratification: Significance of its variable bedding sequences. *Geological Society of America Bulletin*, 93, 663–680.
- Duke, W. L. (1985). Hummocky cross-stratification, tropical hurricanes, and intense winter storms. *Sedimentology*, 32, 167–194.
- Duke, W. L., Arnott, R. W. C., & Cheel, R. J. (1991). Shelf sandstones and hummocky cross-stratification: New insights on a stormy debate. *Geology*, 19, 625–628.
- Dumas, S., & Arnot, R. W. C. (2006). Origin of hummocky and swaley cross-stratification. The controlling influence of unidirectional current strength and aggradation rate. *Geology*, 34, 1073–1076.
- Elez, J., Silva, P. G., Huerta, P., Perucha, M. Á., Civis, J., Roquero, E., Rodríguez-Pascua, M. A., Bardají, T., Giner-Robles, J. L., & Martínez-Graña, A. (2016). Quantitative paleotopography and paleogeography around the Gibraltar arc (South Spain) during the Messinian salinity crisis. *Geomorphology*, 275, 26–45.
- Flinch, J. F., Bally, A. W., & Wu, S. (1996). Emplacement of a passive-margin evaporitic allochthon in the Betic Cordillera of Spain. *Geology*, 24, 67–70.
- Fontana, D., Conti, S., Fioroni, C., & Grillenzoni, C. (2015). Factors controlling the evolution of a wedge-top temperate-type carbonate platform in the Miocene of the northern Apennines (Italy). *Sedimentary Geology*, 319, 13–23.
- Galindo-Zaldívar, J., Braga, J. C., Marín-Lechado, C., Ercilla, G., Martín, J. M., Pedrera, A., Casas, D., Aguirre, J., Ruiz-Constán, A., Estrada, F., Puga-Bernabéu, Á., Sanz de Galdeano, C., Juan, C., García-Alix, A., Vázquez, J. T., & Alonso, B. (2019). Extension in the western Mediterranean. In C. Quesada & J. T. Oliveira (Eds.), *The geology of Iberia: A geodynamic approach* (pp. 61–103). Springer. https://doi.org/10.1007/978-3-030-11190-8_3
- Galindo-Zaldívar, J., Gil, A. J., Borque, M. J., González-Lodeiro, F., Jabaloy, A., Marín-Lechado, C., Ruano, P., & de Galdeano, C. S. (2003). Active faulting in the internal zones of the central Betic cordilleras (SE, Spain). *Journal of Geodynamics*, 36, 239–250.
- Galindo-Zaldívar, J., Ruano, P., Jabaloy, A., & López-Chicano, M. (2000). Kinematics of faults between Subbetic units during the Miocene (central sector of the Betic cordillera). *Comptes Rendus de la Academie Des Sciences de Paris, Sciences de la Terre et Des planètes*, 331, 811–816.
- García-Alix, A., Minwer-Barakat, R., Martín, J. M., Martín-Suárez, E., & Freudenthal, M. (2008). Biostratigraphy and sedimentary evolution of late Miocene and Pliocene continental deposits of the Granada Basin (southern Spain). *Lethaia*, 41, 431–446.
- García-Castellanos, D., Fernández, M., & Torne, M. (2002). Modeling the evolution of the Guadalquivir foreland basin (southern Spain). *Tectonics*, 21, 1018. <https://doi.org/10.1029/2001TC001339>
- García-Hernández, M., López-Garrido, A. C., Rivas, P., Sanz de Galdeano, C., & Vera, J. A. (1980). Mesozoic paleogeographic evolution of the external zones of the Betic Cordillera. *Geologie en Minjbouw*, 59, 155–168.
- González-Castillo, L., Galindo-Zaldívar, J., Pedrera, A., Martínez-Moreno, F. J., & Ruano, P. (2015). Shallow frontal deformation related to active continental subduction: Structure and recent stresses in the westernmost Betic Cordillera. *Terra Nova*, 27, 114–121.
- González-Donoso, J. M., Rodríguez-Fernández, J., Serrano, F., & Vera, J. A. (1980). Precisiones estratigráficas sobre la discordancia intratortonense de Montefrío (Granada). *Boletín de la Real Sociedad Española de Historia Natural (Geología)*, 78, 101–111.
- Hippolyte, J. C., Angelier, J., Roure, F., & Casero, P. (1994). Piggyback basin development and thrust belt evolution: Structural and paleostress analyses of Plio-Quaternary basins in the southern Apennines. *Journal of Structural Geology*, 16, 159–173.
- Hunter, R. E., & Clifton, H. E. (1982). Cyclic deposits and hummocky cross-stratification of probable storm origin in upper cretaceous rocks of Cape Sebastian area, southwestern Oregon. *Journal of Sedimentary Petrology*, 52, 127–144.
- Hurst, A., Scott, A., & Vigorito, M. (2011). Physical characteristics of sand injectites. *Earth-Science Reviews*, 106, 215–246.
- Ingersoll, R. V. (2012). Tectonics of sedimentary basins, with revised nomenclature. In C. Busby & A. Azor (Eds.), *Tectonics of sedimentary basins: Recent advances*. Blackwell Publishing Ltd.
- Jabaloy, A., Galindo-Zaldívar, J., & González-Lodeiro, F. (1992). The Mecina extensional system: Its relation with the post-Aquitania piggy-back basins and the paleostresses evolution (Betic cordilleras, Spain). *Geo-Marine Letters*, 12, 96–103.
- Jabaloy, A., Martín-Algarra, A., Padrón-Navarta, J. A., Martín-Martín, M., Gómez-Pugnaire, M. T., López Sánchez-Vizcaíno, V., & Garrido, C. J. (2019). Lithological successions of the internal zones and flysch trough units of the Betic chain. In C. Quesada & J. T. Oliveira (Eds.), *The geology of Iberia: A geodynamic approach. Regional Geology Reviews*. Springer. https://doi.org/10.1007/978-3-030-11295-0_8
- James, N. P. (1997). The cool-water carbonate depositional realm. In N. P. James & A. D. Clarke (Eds.), *Cool water carbonates* (Vol. 56, pp. 1–20). SEPM Special Publication.
- Jones, A. P., & Omoto, K. (2000). Towards establishing criteria for identifying trigger mechanisms for soft-sediment deformation: A case study of late Pleistocene lacustrine sands and clays, Onikobe and Nakayamadaira basins, northeastern Japan. *Sedimentology*, 47, 1211–1226.
- Kawakami, G. (2013). Foreland basins at the Miocene arc-arc junction, Central Hokkaido, northern Japan. In Y. Itoh (Ed.), *Mechanism of sedimentary basin formation*. Multidisciplinary approach on active plate margins.
- Larrasoña, J., Sierro, F. J., Mata, M. P., van den Berg, B. C. J., Pérez-Asensio, J. N., Salazar, Á., Salvany, J. M., Ledesma, S., García-Castellanos, D., Civis, J., & Cunha, P. (2019). Guadalquivir Basin. In C. Quesada & T. Olivira (Eds.), *The geology of Iberia: A geodynamic approach. Volume 4: Cenozoic basins* (pp. 40–59). Springer.
- Ledesma, S. M. (2000). *Astrobiocronología y estratigrafía de alta resolución del Neógeno de la Cuenca del Guadalquivir-Golfo de Cádiz*. Ph.D. Thesis. Universidad de Salamanca.
- Lirer, F., Foresi, L. M., Iaccarino, S. M., Salvatorini, G., Turco, E., Cosentino, C., Sierro, F. J., & Caruso, A. (2019). Mediterranean Neogene planktonic foraminifer biozonation and biochronology. *Earth-Science Reviews*, 196, 102869. <https://doi.org/10.1016/j.earscirev.2019.05.013>
- Longhitano, S. G. (2018). Between Scylla and Charybdis (part 1): The sedimentary dynamics of the modern Messina Strait (central Mediterranean) as analogue to interpret the past. *Earth-Science Reviews*, 185, 259–287.
- Lupiani-Moreno, E., & Soria-Mingorance, J. (1985). *Montefrío. Mapa geológico de España, escala 1:50.000*. Instituto Geológico y Minero de España.
- Martín, J. M., Braga, J. C., Aguirre, J., & Betzler, C. (2004). Contrasting models of temperate carbonate sedimentation in a small

- Mediterranean embayment: The Pliocene Carboneras basin, SE Spain. *Journal of the Geological Society of London*, 161, 387–399.
- Martín, J. M., Braga, J. C., Aguirre, J., & Puga-Bernabéu, Á. (2009). History and evolution of the north-Betic Strait (Prebetic zone, Betic cordillera): A narrow, early Tortonian, tidal-dominated, Atlantic–Mediterranean marine passage. *Sedimentary Geology*, 216, 80–90.
- Martín, J. M., Braga, J. C., & Betzler, C. (2001). The Messinian Guadalhorce corridor: The last northern, Atlantic–Mediterranean gateway. *Terra Nova*, 13, 418–424.
- Martín, J. M., Braga, J. C., Betzler, C., & Brachert, T. C. (1996). Sedimentary model and high-frequency cyclicity in a Mediterranean, shallow-shelf, temperate – Carbonate environment (uppermost Miocene, Agua Amarga Basin, southern Spain). *Sedimentology*, 43, 263–277.
- Martín, J. M., Puga-Bernabéu, Á., Aguirre, J., & Braga, J. C. (2014). Miocene Atlantic–Mediterranean seaways in the Betic Cordillera (southern Spain). *Revista de la Sociedad Geológica de España*, 27, 175–186.
- Martínez del Olmo, W. (2019). El complejo olistostrómico del Mioceno de la Cuenca del Río Guadalquivir (SO de España). *Revista de la Sociedad Geológica de España*, 32, 3–16.
- Martínez del Olmo, W., García Mallo, J., Leret Verdú, G., Serrano, A., & Suárez, J. (1984). Modelo tectosedimentario del Bajo Guadalquivir. *I Congreso Geológico de España. Segovia*, 1, 199–213.
- Martínez del Olmo, W., & Martín, D. (2016). El Neógeno de la cuenca Guadalquivir–Cádiz (Sur de España). *Revista de la Sociedad Geológica de España*, 29, 35–58.
- Martín-Serrano, Á. (1986). *Antequera. Segunda serie – Primera edición. Mapa geológico de España, escala 1:50.000*. Instituto Geológico y Minero de España.
- Milliman, J. D., & Syvitski, J. P. M. (1992). Geomorphic/tectonic control of sediment discharges to the ocean: The importance of small mountains rivers. *Journal of Geology*, 100, 525–544.
- Mount, J. F. (1982). Storm-surge-ebb origin of hummocky cross-stratified units of the Andrews Mountain member, Campito formation (lower Cambrian), white-Inyo Mountains, eastern California. *Journal of Sedimentary Petrology*, 52, 951–958.
- Murray, J. W. (2006). *Ecology and applications of benthic foraminifera*. Cambridge University Press.
- Mutti, E., Davoli, G., Tinterri, R., & Zavala, C. (1996). The importance of fluvio-deltaic systems dominated by catastrophic flooding in tectonically active basins. *Memorie di Scienze Geologiche*, 48, 233–291.
- Mutti, E., Tinterri, R., Benevelli, G., di Biase, D., & Cavanna, G. (2003). Deltaic, mixed and turbidite sedimentation of ancient foreland basins. *Marine and Petroleum Geology*, 20, 733–755.
- Obermeier, S. F. (1996). Use of liquefaction-induced features for paleoseismic analysis. An overview of how seismic liquefaction features can be distinguished from other features and how their regional distribution and properties of source sediment can be used to infer the location and strength of Holocene paleo-earthquakes. *Engineering Geology*, 44, 1–76.
- Ori, G. G., & Friend, P. F. (1984). Sedimentary basins formed and carried piggyback on active thrust sheets. *Geology*, 12, 475–478.
- Owen, G., & Moretti, M. (2011). Identifying triggers for liquefaction-induced soft-sediment deformation in sands. *Sedimentary Geology*, 235, 141–147.
- Pedraza, A., Marín-Lechado, C., Martos-Rosillo, S., & Roldán, F. J. (2012). Curved fold-and-thrust accretion during the extrusion of a synorogenic viscous allochthonous sheet: The Estepa range (external zones, Western Betic cordillera, Spain). *Tectonics*, 31, Article TC4013. <https://doi.org/10.1029/2012TC003119>
- Pérez-Asensio, J. N., Aguirre, J., Jiménez-Moreno, G., Schmiedl, G., & Civis, J. (2013). Glacioeustatic control on the origin and cessation of the Messinian salinity crisis. *Global and Planetary Change*, 111, 1–8.
- Pérez-Asensio, J. N., Aguirre, J., Schmiedl, G., & Civis, J. (2012). Impact of restriction of the Atlantic–Mediterranean gateway on the Mediterranean outflow water and eastern Atlantic circulation during the Messinian. *Paleoceanography*, 27, PA3222. <https://doi.org/10.1029/2012PA002309>
- Pérez-López, A., & Sanz de Galdeano, C. (1994). Tectónica de los materiales triásicos en el sector central de la Zona Subbética (Cordillera Bética). *Revista de la Sociedad Geológica de España*, 7, 141–153.
- Pérez-Valera, F., Sánchez-Gómez, M., Pérez-López, A., & Pérez-Valera, L. A. (2017). An evaporite-bearing accretionary complex in the northern front of the Betic-Rif orogen. *Tectonics*, 36, 1006–1036. <https://doi.org/10.1002/2016TC004414>
- Peyre, Y. (1974). *Géologie d'Antequera et de sa région (Cordillères Bétiques, Espagne)*. Dissertation. University of Paris.
- Platt, J. P., Behr, W. M., Johanesen, K., & Williams, J. R. (2013). The Betic-Rif arc and its orogenic hinterland: A review. *Annual Review of Earth and Planetary Sciences*, 41, 313–357.
- Postman, G., Cartigny, M., & Kleverlaan, K. (2009). Structureless, coarse-tail graded Bouma Ta formed by internal hydraulic jump of the turbidity current? *Sedimentary Geology*, 219, 1–6.
- Puga-Bernabéu, Á., Braga, J. C., Aguirre, J., & Martín, J. M. (2023). Sedimentary dynamics and topographic controls on the tidal-dominated Zagra Strait, early Tortonian, Betic Cordillera. In V. M. Rossi, S. G. Longhitano, C. Olariu, & F. Chiocci (Eds.), *Straits and seaways: Controls, processes and implications in modern and ancient systems* (Vol. 523, pp. 427–451). Geological Society of London, Special Publication. <https://doi.org/10.1144/SP523-2021-85>
- Puga-Bernabéu, Á., Braga, J. C., & Martín, J. M. (2007). High-frequency cycles in upper-Miocene ramp-temperate carbonates (Sorbas Basin, SE Spain). *Facies*, 53, 329–345.
- Puga-Bernabéu, Á., Martín, J. M., & Braga, J. C. (2008). Sedimentary processes in a submarine canyon excavated into a temperate-carbonate ramp (Granada Basin, southern Spain). *Sedimentology*, 55, 1449–1466.
- Puga-Bernabéu, Á., Martín, J. M., Braga, J. C., & Aguirre, J. (2014). Offshore remobilization processes and deposits in low-energy temperate-water carbonate-ramp systems: Examples from the Neogene basins of the Betic Cordillera (SE Spain). *Sedimentary Geology*, 304, 11–27.
- Reolid, J., Aguirre, J., Pérez-Asensio, J. N., Puga-Bernabéu, Á., Braga, J. C., & Martín, J. M. (2022). Mixed carbonate-siliciclastic contourite drift deposits associated with the entrance of an Atlantic–Mediterranean corridor (late Miocene, southwest Spain). *Sedimentary Geology*, 439, 106233. <https://doi.org/10.1016/j.sedgeo.2022.106233>
- Rodríguez-Fernández, J. (1982). *El Mioceno del sector central de las Cordilleras Béticas*. Ph.D. Thesis. Universidad de Granada.
- Rodríguez-Fernández, J., Azor, A., & Azañón, J. M. (2012). The Betic intramontane basins (SE Spain): Stratigraphy, subsidence, and tectonic history. In C. Busby & A. Azor (Eds.), *Tectonics of sedimentary basins: Recent advances* (pp. 461–479). Blackwell Publishing Ltd.

- Rodríguez-Fernández, J., Roldán, F. J., Azañón, J. M., & García-Cortés, A. (2013). El colapso gravitacional del frente orogénico alpino en el Dominio Subbético durante el Mioceno medio-superior: el complejo extensional Subbético. *Boletín Geológico y Minero de España*, *124*, 477–504.
- Roldán, F. J. (1995). *Evolución Neógena de la Cuenca del Guadalquivir*. Ph.D. Thesis. Universidad de Granada.
- Roldán, F. J. (2009). Olistostrome units of the Betic foreland. In A. García-Cortés (Ed.), *Spanish geological frameworks and geosites* (pp. 124–131). An approach to Spanish geological heritage of international relevance.
- Roldán, F. J., Galindo-Zaldívar, J., Ruano, P., Chalouan, A., Pedrera, A., Ahmamous, M., Ruiz-Constán, A., Sanz de Galdeano, C., Benmakhoulouf, M., López-Garrido, Á. C., Anahnah, F., & González-Castillo, L. (2014). Basin evolution associated to curved thrusts: The Prerif ridges in the Volubilis area (Rif cordillera, Morocco). *Journal of Geodynamics*, *77*, 56–69.
- Roldán, F. J., & Rodríguez-Fernández, J. (1991). Un ejemplo de cuenca de piggy-back asociada a la evolución neógena del frente de las Zonas Externas Béticas. *Congreso Grupo Español del Terciario*, *1*, 297–300.
- Rossi, V. M., Longhitano, S. G., Olariu, C., & Chiocci, F. L. (2023). Straits and seaways: Controls, processes and implications in modern and ancient systems. In V. M. Rossi, S. G. Longhitano, C. Olariu, & F. Chiocci (Eds.), *Straits and seaways: Controls, processes and implications in modern and ancient systems* (Vol. 523, pp. 1–13). Geological Society of London, Special Publication. <https://doi.org/10.1144/SP523-2021-85>
- Ruiz-Constán, A., Galindo-Zaldívar, J., Pedrera, A., & Sanz de Galdeano, C. (2009). Gravity anomalies and orthogonal box fold development on heterogeneous basement in the Neogene Ronda depression (Western Betic Cordillera). *Journal of Geodynamics*, *47*, 210–217.
- Ruiz-Constán, A., Pedrera, A., Galindo-Zaldívar, J., Pous, J., Arzate, J., Roldán, F. J., Marín-Lechado, C., & Anahnah, F. (2012). Constraints on the frontal crustal structure of a continental collision from an integrated geophysical research: The central-western Betic cordillera (SW Spain). *Geochemistry, Geophysics, Geosystems*, *13*, Q08012. <https://doi.org/10.1029/2012GC004153>
- Sanz de Galdeano, C. (1990). Geologic evolution of the Betic cordilleras in the Western Mediterranean, Miocene to the present. *Tectonophysics*, *172*, 107–119.
- Sanz de Galdeano, C., & Alfaro, P. (2004). Tectonic significance of the present relief of the Betic Cordillera. *Geomorphology*, *63*, 175–190.
- Sanz de Galdeano, C., & López Garrido, Á. C. (2012). The Torcal de Antequera, an example of a structure formed by a large scale dextral transcurrent system. *Estudios Geológicos*, *68*, 189–202.
- Sanz de Galdeano, C., Lozano, J. A., & Puga, E. (2008). El “Trias de Antequera”: naturaleza, origen y estructura. *Revista de la Sociedad Geológica de España*, *21*, 110–124.
- Sanz de Galdeano, C., & Vera, J. A. (1992). Stratigraphic record and palaeogeographical context of the Neogene basins in the Betic cordillera, Spain. *Basin Research*, *4*, 21–36.
- Serrano, F. (1979). *Los foraminíferos planctónicos del Mioceno superior de la cuenca de Ronda y su comparación con los de otras áreas de las Cordilleras Béticas*. Ph.D. Thesis. Universidad de Málaga.
- Shanmugam, G. (2021). Soft-sediment deformation structures. In G. Shanmugam (Ed.), *Mass transport, gravity flows, and bottom currents* (pp. 377–439). Elsevier.
- Sierro, F. J., González-Delgado, J. A., Dabrio, C. J., Flores, J. A., & Civis, J. (1996). Late Neogene depositional sequences in the foreland basin of Guadalquivir (SW Spain). In P. Friend & C. J. Dabrio (Eds.), *Tertiary basins of Spain* (pp. 339–345). Cambridge University Press.
- Sinclair, H. D. (1997). Tectonostratigraphic model for underfilled peripheral foreland basins: An alpine perspective. *Geological Society of America Bulletin*, *109*, 324–346.
- Targhi, S., Barhoun, N., Taiufiq, N. B., Achab, M., Essamoud, R., Bahaj, H., Rahmouna, J., & Berry, N. (2023). Late Miocene biostratigraphy and paleoenvironment of the Sais Basin (southern Rifian corridor, Morocco): New insights from the Moulay Yakoub area. *Carnets de Geologie*, *23*, 53–75.
- Topal, S., & Özkul, M. (2014). Soft-sediment deformation structures interpreted as seismites in the Kolankaya formation, Denizli Basin (SW Turkey). *The Scientific World Journal*, *2014*, 1–13. <https://doi.org/10.1155/2014/352654>
- Tulbure, M. A., Capella, W., Barhoun, N., Flores, J. A., Hilgen, F. J., Krijgsman, W., Kouenhoven, T., Sierro, F. J., & Yousfi, M. Z. (2017). Age refinement and basin evolution of the north Rifian corridor (Morocco): No evidence for a marine connection during the Messinian salinity crisis. *Palaeogeography, Palaeoclimatology, Palaeoecology*, *485*, 416–432.
- van der Schee, M., van den Berg, B. C. J., Capella, W., Simon, D., Sierro, F. J., & Krijgsman, W. (2018). New age constraints on the western Betic intramontane basins: A late Tortonian closure of the Guadalhorce corridor? *Terra Nova*, *30*, 325–332.
- Vera, J. A., & González-Donoso, J. M. (1964). Discordancia intravindobonense en Montefrío, Zona Subbética (provincial de Granada). *Noticias y Comunicaciones del Instituto Geológico y Minero de España*, *76*, 19–32.
- Zabala, C. (2020). Hyperpycnal (over density) flows and deposits. *Journal of Palaeogeography*, *9*, 21. <https://doi.org/10.1186/s42501-020-00065-x>
- Zamanian, K., Pustovoytov, K., & Kuzyakov, Y. (2016). Pedogenic carbonates: Forms and formation processes. *Earth-Science Reviews*, *157*, 1–17.

SUPPORTING INFORMATION

Additional supporting information can be found online in the Supporting Information section at the end of this article.

How to cite this article: Aguirre, J., Braga, J. C., Martín, J. M., & Puga-Bernabéu, Á. (2024). Tectonic control on the palaeogeographic evolution of thrust-top basins at the active margin of the Guadalquivir Basin (central Betic Cordillera, S Spain). *Basin Research*, *36*, e12847. <https://doi.org/10.1111/bre.12847>